Internal boundaries of the loop amplituhedron

Gabriele Dian, Paul Heslop and Alastair Stewart

Mathematics Department, Durham University, Science Laboratories,
South Rd, Durham DH1 3LE

Abstract

The strict definition of positive geometry implies that all maximal residues of its canonical form are ±1. We observe, however, that the loop integrand of the amplitude in planar $\mathcal{N} = 4$ super Yang-Mills has maximal residues not equal to ±1. We find the reason for this is that deep in the boundary structure of the loop amplituhedron there are geometries which contain internal boundaries: codimension one defects separating two regions of opposite orientation. This phenomenon requires a generalisation of the concept of positive geometry and canonical form to include such internal boundaries and also suggests the utility of a further generalisation to 'weighted positive geometries'. We re-examine the deepest cut of $\mathcal{N} = 4$ amplitudes in light of this and obtain new all order residues.

Contents

1 Introduction

The amplituhedron is a geometrical object introduced in [1,2] and was discovered to yield a beautiful intrinsic definition of the perturbative expansion of planar amplitudes in $\mathcal{N} = 4$ super Yang-Mills (SYM), allowing for entirely novel expressions for amplitudes to be found (see [3] for a review). In this framework, amplitude integrands are obtained as a differential form, called the canonical form, of the amplituhedron. The boundary structure of the amplituhedron then encodes the full singularity structure of the integrand. More precisely, residues of the amplitude are the canonical forms of the corresponding amplituhedron boundaries, which recursively give further residues as boundaries of the boundaries etc. Thus the amplituhedron provides a fascinating way to analyse the singularity structure of amplitude integrands, which in turn is intimately connected to the branch cut structure of the integrated amplitude [4,5]. In this paper, we investigate multiple residues of amplitudes and the corresponding amplituhedron boundary structure. In particular, we point out new features which have not been appreciated previously.

First, we note that a direct consequence of amplitudes arising from positive geometries is that the amplitude should have unit maximal residues. This arises geometrically simply from the fact that maximal residues correspond to dimension 0 geometries, ie points, which can only differ by their orientation. Tree-level amplitudes indeed appear to have unit maximal residues. The tree level superamplitudes can be computed by summing a certain set of on-shell diagrams [6] arising from the BCFW recursion relation [7]. The on-shell diagrams manifestly have only logarithmic singularities and non-vanishing maximal residues equal to ± 1 and have a natural geometric interpretation in amplituhedron space [1]. It was recently proven that they provide a tessellation of the amplituhedron [8] and it would be interesting to see if the details of this proof can also be used to prove that the non-vanishing maximal residues only equal ± 1.[1]

What we will observe however is that, unlike at tree level, the maximal residues of the *loop* amplitude integrand take many different values in $\mathbb{Z}$. Examining the corresponding geometry, the loop amplituhedron, we find starting from 2 loops that it contains a novel feature, namely *internal boundaries*, deep within its boundary structure and find these are the geometric source
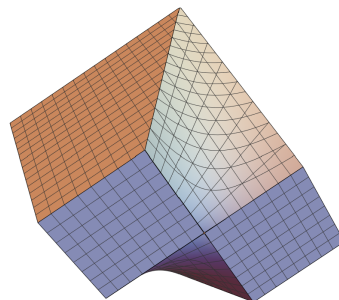
---

[1]It does not automatically follow since there are simple examples of geometries which can be tessellated with positive geometries but which themselves are not positive geometries, as we will see.

of the non-unit residues. By an internal boundary we mean a codimension 1 surface separating two regions of opposite orientation, as below:

internal boundary:

We emphasise that such internal boundaries do not appear in the amplituhedron itself, but deep within its boundary structure. That is, we claim that a certain boundary component of a boundary component of a...of the amplituhedron will contain an internal boundary.

There has been tremendous progress in understanding the geometry of the tree level amplituhedron and its canonical form [8, 12–15]. The loop amplituhedron and its tilings on the other hand are much less well understood. A first exploration of the boundaries of the MHV loop amplituhedron was started in [2], where the 2-loop MHV amplitude was computed by triangulating the amplituhedron and several cuts were discussed. Then a systematic investigation of the boundaries of the MHV loop amplituhedron was carried out up to four loops in [16] and extended to negative mutual positivity conditions in [17]. Internal boundaries, however, appear to have been missed in the construction of the stratification of the loop amplituhedron in previous works. One possible reason for this is that these boundaries cannot be labelled by the Plücker coordinates that are naturally used to describe the amplituhedron: $\langle Yijkl \rangle$, $\langle ABij \rangle$ and $\langle A_i B_i A_j B_j \rangle$. For example, internal boundaries arise when computing the all-in-one-point cut of [18] via consecutive single residues. By carefully looking at the boundary corresponding to three loop lines $(A_1 B_1), (A_2 B_2), (A_3 B_3)$ all intersecting the point A, one finds that $\langle AB_1 B_2 B_3 \rangle = 0$ represents an internal boundary.

We find that the internal boundaries appear to be closely associated with 'composite singularities' (see [9]). A simple example of a composite singularity is given by $2/(z(z + xy))$. This only has two factors, but when taking the residue at $z = 0$ the irreducible factor $z + xy$ factorises to xy. Indeed the above is the canonical form of the ordinary looking geometry given by points in 3d satisfying $z > 0, z + xy > 0$, which pictured from below looks like the following:

This geometry contains a boundary (nearest to the viewer in the above picture) at $z = 0$, which is given by $xy > 0$; two opposite quadrants of a plane. This 2d boundary in turn has a boundary at $y = 0$, consisting of two 1-dimensional regions $x > 0, x < 0$ with opposite orientation. Finally, this 1d region contains a 0-dimensional internal boundary at $x = 0$. This type of structure appears in the boundaries of the loop amplituhedron, implying that the loop amplituhedron is not a 'positive geometry' in the sense usually understood [10].[2]

---

[2] Note that maximal residues differing from ±1 have been observed previously in the square of the super amplitude, where they appear already at tree level [11]. In fact, there they appear in a less subtle way geometrically: the tree squared amplituhedron interior is disconnected and internal boundaries correspond to boundaries shared between the different connected components, whereas the loop amplituhedron interior is connected.

We conclude that we need to generalise the definition of 'positive geometry' to allow for such internal boundaries and to incorporate the loop amplituhedron. Thus, we define *generalised positive geometries* (GPGs) which include internal boundaries. Then we introduce a corresponding extension of the recursive definition of the canonical form, by adding an additional term for internal boundaries which should appear with a factor of 2. In doing so, the loop level amplitude can still be obtained as the canonical form of the amplituhedron geometry.
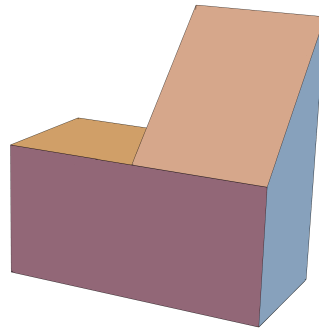
In practise, the most convenient way to compute canonical forms of positive geometries is via tessellation (eg via cylindrical decomposition) rather than explicit use of the recursive definition. It is important to note that tessellations work for these generalised positive geometries (GPGs) just as for positive geometries. The canonical form of a GPG can be computed simply by summing over the canonical forms of the tiles in a tessellation. Indeed, the space of GPGs is closed under the disjoint-union: any geometry that can be tiled in GPGs is itself a GPG. This differs from positive geometries, which are incomplete under tessellation. We will see examples of geometries that can be tessellated in positive geometries, but which are not themselves a positive geometry.

While the above generalisation of positive geometry to include internal boundaries is perfectly adequate to deal with the loop amplituhedron, it immediately suggests an even more general type of geometry which may be of wider use, namely 'weighted positive geometry'. Any oriented geometry is defined by specifying a region (the geometry) together with its orientation form. However, in order to compute the canonical form of a geometry containing internal boundaries, such as the loop amplituhedron, one needs some extra information encoding which points belong to an external boundary and which belong to an internal boundary. It then seems very natural to define a new object called the weighted geometry (WG). A WG is given by a pair (w, O), where w is an integer valued function we call the weight function and O is the orientation form. The value of the weight function on a point intuitively represents the number of coinciding oriented geometries at that point. For example, an ordinary oriented geometry $X_{\geq 0}$ can be described as a weighed geometry with weight function $w(x) = 1$ for all $x \in X_{\geq 0}$ and zero elsewhere, while an internal boundary will have $w(x) = 2$ instead (an internal boundary can be viewed as two external boundaries coinciding).

The space of weighted geometries is naturally equipped with two key operators: a sum and a projection onto boundary. The sum generalizes the union of disconnected oriented geometries by allowing for overlaps (the weights on the overlap simply sum). The projection onto boundary operator instead allows one to define the induced weight function and orientation on the boundary of a WG. As a consequence, boundaries of WGs are WGs. This construction allows for a recursive definition of the canonical form and weighted positive geometries (WPG), that treats internal and external boundaries on the same footing and makes the tiling properties of the canonical form trivial. In fact, the canonical form turns out to be a linear operator with respect to the sum of WPGs. Then, because a tiling of a geometry $X_{\geq 0}$ in this new language is nothing but a sum of WPGs, it follows trivially that the canonical form of a sum (union) of WPGs is equal to the sum of the canonical forms.

Another feature of the geometry of the amplituhedron which seems to have not been emphasised in the literature previously is the geometrical equivalent of the fact that multiple residues are not in general uniquely defined. One way to define multiple residues is via the residue form [19] (see also [9]) which essentially defines it via a sequence of single residues. However, taking these in different orders can give completely different results. There is a direct analogue of this fact in terms of taking boundaries of the corresponding geometry. Rather than talking about codimension 2 boundary components, instead it is the precise boundary component of the boundary component which will give the multiple residue defined by taking the corresponding simple poles in sequence. Taking these boundary components in different orders can give different results.

Consider the solid 3d geometry below, which will serve as a very simple example to illustrate the dependence on the order of taking boundaries.

Here we have a 3d shape which looks like a house with a flat roof on the left and an angled roof on the right. The planes in which the two roofs lie intersect along the top of the front wall which we will call the 'front eaves'. While one might wish to talk about the codimension two boundary component corresponding to the entire front eaves, taking appropriate boundaries of boundaries can give results which differ from this. One could first take the flat roof boundary component and then take the front eave boundary of that. This results in only the left half of the front eaves. If on the other hand we first take the slanted roof boundary component and then the font eaves boundary of that, we obtain the right half of the front eaves. Finally we could instead first take the boundary component on the front wall, and then the boundary component of that at the top, resulting in the entire length of the front eaves. We thus arrive at three different results from taking a sequence of boundary components.

This is completely consistent with what we get from multiple residues. Indeed, this example can be made completely precise and the corresponding canonical form and residues taken. We choose coordinates such that the flat roof lies on the plane $z = 0$, the slanted roof on $y = z$ and the front wall $y = 0$ (we also put the two side walls at $x = -1, x = 1$, the back wall at $y = 1$ and the floor at $z = -1$). The corresponding canonical form, which can easily be obtained by summing the canonical form of the living space and the roof, is

$$\Omega = \frac{1}{(x-1)x(y-1)z(y-z)} - \frac{2}{(x-1)(x+1)(y-1)yz(z+1)}. \tag{1}$$

The residue corresponding to the front boundary of the flat roof is $\mathrm{Res}_{y=0}\mathrm{Res}_{z=0}\Omega = -dx/(x(x+1)) = \Omega[-1, 0]$, which is the canonical form of the one dimensional interval $-1 \leq x \leq 0$. On the other hand, the residue corresponding to the front boundary of the slanted roof is $\mathrm{Res}_{y=0}\mathrm{Res}_{z=y}\Omega = -dx/(x(x-1)) = \Omega[0, 1]$, the canonical form of the one dimensional interval $0 \leq x \leq 1$. Finally, the residue corresponding to the top boundary of the front wall is $\mathrm{Res}_{z=0}\mathrm{Res}_{y=0}\Omega = 2dx/((x-1)(x+1)) = \Omega[1, -1]$. All cases correspond in the end to the codimension two line $z = 0, y = 0$ but the precise way we get there gives different results.

Another example of this phenomenon is the case of all l loop lines intersecting in a single point, which is a configuration closely related to the deepest cut of [18]. At 4 points, from 4 loops onward, different orderings of single residues give algebraically different results, as we will show in section 4.3. With this in mind, we do a detailed analysis of the all-in-one-point cut and find quite a complicated structure in general, although it seems one can always keep taking further loop loop residues to reduce to the 3 loop all-in-one-point-and-plane cut.

This paper is structured as follows. In section 2 we present a simple example of a maximal residue at two loops equal to ± 2 rather than ± 1, and give its geometrical interpretation as an internal boundary. In section 3 we formally define generalized positive geometries (GPGs),

which allow internal boundaries, and their canonical forms. We discuss tilings of GPGs and the key property that *any* geometry that can be triangulated by GPGs is a GPG, a property not shared by positive geometries. We describe the algebraic cylindrical decomposition algorithm, originally presented in [20], to compute the canonical form, and use it to identify a class of GPGs. Then, we introduce a generalisation of GPGs which we call weighted positive geometries. In section 4 we turn our attention to a specific boundary of the loop amplituhedron, that is the all-in-one-point cut, and we compute its geometry and discuss its internal boundary. Finally, in section 5 we take further cuts on the result of the all-in-one-point cut and obtain a new all loop formula.

2 Two loop maximal cuts and internal boundaries

The purpose of this section is to show that the loop level amplitude can have maximal residues which are not $\pm 1, 0$ and give the geometrical interpretation of this fact. Consider the four point two-loop MHV amplitude integrand written as a volume form in momentum twistor space

$$
\text{MHV}(2) = \frac{\langle A_1B_1\mathrm{d}^2A_1\rangle\langle A_1B_1\mathrm{d}^2B_1\rangle\langle A_2B_2\mathrm{d}^2A_2\rangle\langle A_2B_2\mathrm{d}^2B_2\rangle\langle 1234\rangle^3}{\langle A_1B_1A_2B_2\rangle\langle A_1B_114\rangle\langle A_1B_112\rangle\langle A_2B_223\rangle\langle A_2B_234\rangle}
$$
$$
\times\left[\frac{1}{\langle A_1B_134\rangle\langle A_2B_212\rangle} + \frac{1}{\langle A_1B_123\rangle\langle A_2B_214\rangle}\right] \quad + \quad A_1B_1 \leftrightarrow A_2B_2. \quad (2)
$$

Here we have external momentum twistors $Z_1, .., Z_4 \in \mathbb{C}^4$ and loop integration variables $A_iB_i \in \mathbb{C}^4$ which define a plane through the origin $aA_i + bB_i \in \mathbb{C}^4$ i.e. a line in projective twistor space. The bracket notation denotes the determinant of the 4×4 matrix formed by taking the four twistors inside as columns. We also surpress the Zs, so eg $\langle A_1B_112\rangle := \det(A_1, B_1, Z_1, Z_2)$.

Now we compute the multi-residue corresponding to taking a sequence of residues on

$$
\langle A_1B_112\rangle = 0, \quad \langle A_1B_134\rangle = 0, \quad \langle A_2B_212\rangle = 0, \quad \langle A_2B_234\rangle = 0, \quad \langle A_1B_1A_2B_2\rangle = 0, \quad (3)
$$

followed by a residue on a hidden pole which appears at $\langle 12B_1B_2\rangle = 0$. To do this we first parametrise the $4{\times}4$ $Z = (Z_1Z_2Z_3Z_4)$ matrix as the identity and the loops as

$$
\begin{pmatrix} A_i \\ B_i \end{pmatrix} = \begin{pmatrix} 1 & a_i & 0 & -b_i \\ 0 & c_i & 1 & d_i \end{pmatrix}. \quad (4)
$$

For this choice, the brackets read

$$
\langle A_iB_i12\rangle = b_i, \quad \langle A_iB_i23\rangle = d_i, \quad \langle A_iB_i34\rangle = c_i, \quad \langle A_iB_i14\rangle = a_i,
$$
$$
\langle A_1B_1A_2B_2\rangle = -(b_1-b_2)(c_1-c_2)-(a_1-a_2)(d_1-d_2), \quad \langle 1234\rangle = 1, \quad (5)
$$
$$
\langle A_iB_i\mathrm{d}^2A_i\rangle\langle A_iB_i\mathrm{d}^2B_i\rangle = \mathrm{d}a_i\mathrm{d}b_i\mathrm{d}c_i\mathrm{d}d_i.
$$

Omitting the differentials, the amplitude (2) in these coordinates reads

$$
\text{MHV}(2) = -\frac{a_2d_1 + a_1d_2 + b_2c_1 + b_1c_2}{a_1a_2b_1b_2c_1c_2d_1d_2\left((a_1-a_2)(d_1-d_2)+(b_1-b_2)(c_1-c_2)\right)}. \quad (6)
$$

Now we take the first four residues in (3), namely $b_1 = 0, c_1 = 0, b_2 = 0, c_2 = 0$. We see that the complicated factor in the denominator factorises thus revealing a new pole,[3] giving

$$
-\frac{a_2d_1 + a_1d_2}{a_1a_2d_1d_2(a_1-a_2)(d_1-d_2)}. \quad (7)
$$

---

[3]Such poles have been observed in the amplitude previously, and have been dubbed composite residues [9]. See also the example in the introduction.

Then we take the residue in a_1 at $a_1 = a_2$, obtaining

$$-\frac{(d_1 + d_2)}{a_2 d_1 d_2 (d_1 - d_2)}. \tag{8}$$

We continue by taking the residue in d_1 at $d_1 = d_2$, obtaining

$$-\frac{2}{a_2 d_2}, \tag{9}$$

up to an overall sign due to the ordering of the differential $d^2 a_i d^2 b_i d^2 c_i d^2 d_i$. From (9), it is clear that this form has maximal residues equal to ± 2, contradicting the consequence of this being the canonical form of a positive geometry.
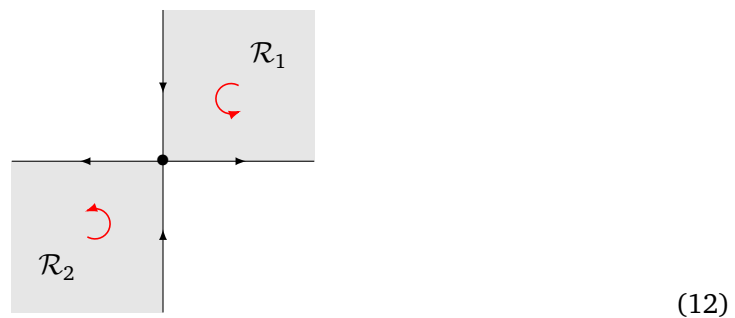
Geometrical interpretation

Let's try to understand how this factor of two appears geometrically from the amplituhedron. First we take boundaries corresponding to the four residues at $\{\langle A_1 B_1 12\rangle = 0, \langle A_1 B_1 34\rangle = 0, \langle A_2 B_2 12\rangle = 0, \langle A_2 B_2 34\rangle = 0\}$. The order in which these are performed is not important and the resulting geometry has each loop line $(A_i B_i)$ described by a point A_i in the segment $\overline{12}$ and a point B_i in $\overline{34}$, together with a further mutual positivity condition $\langle A_1 B_1 A_2 B_2\rangle > 0$. It is natural then to parametrise A_i, B_i as $A_i = Z_1 + a_i Z_2$ and $B_i = Z_3 + d_i Z_4$, so that the geometry is described by the inequalities

$$a_i > 0, \quad d_i > 0, \quad -(a_1 - a_2)(d_1 - d_2) > 0. \tag{10}$$

Notice that the mutual positivity inequality factorizes in to the product of two terms $a_1 > a_2, d_1 < d_2$ or $a_1 < a_2, d_1 > d_2$. This is just the geometrical version of composite residues mentioned in the introduction and above (7). The factorisation results in a corresponding geometry given by two regions

$$\mathcal{R}_1 := \{a_1, a_2, d_1, d_2 \mid a_1 > a_2 > 0 \wedge d_2 > d_1 > 0\},$$
$$\mathcal{R}_2 := \{a_1, a_2, d_1, d_2 \mid a_2 > a_1 > 0 \wedge d_1 > d_2 > 0\}. \tag{11}$$

This geometry is illustrated in the following picture,

$$\tag{12}$$

where the x axis corresponds to increasing $a_1 - a_2$ and the y axis increasing $d_2 - d_1$.

The two regions share only a codimension 2 boundary that is contained on the surface $(a_1 - a_2) = 0, (d_1 - d_2) = 0$. Both regions $\mathcal{R}_1, \mathcal{R}_2$ come equipped with an orientation induced by the bulk geometry, which in this case is the same for both regions. Each of the two regions is clearly a positive geometry, with canonical forms

$$\Omega(\mathcal{R}_1) = -\frac{1}{a_1 d_2 (a_1 - a_2)(d_1 - d_2)},$$
$$\Omega(\mathcal{R}_2) = -\frac{1}{a_2 d_1 (a_2 - a_1)(d_2 - d_1)}. \tag{13}$$

The sum of these correctly reproduces the corresponding residue of the amplitude (7). Since the two regions share a lower codimension boundary we have to see what happens on this boundary to decide if the union is or isn't a positive geometry. We can consider for example the $(d_2 - d_1) = 0$ boundary by sending $d_2 \to d_1$. This corresponds to projecting onto the x axis of (12) and thus looks as

$$\xleftarrow{\hspace{3cm}} \bullet \xrightarrow{\hspace{3cm}}$$
$$\mathcal{R}'_2 \qquad\qquad\qquad\qquad \mathcal{R}'_1 \qquad\qquad\qquad (14)$$

We again get two regions

$$\mathcal{R'}_1 := \{a_1, a_2, d_1 \mid d_1 > 0 \wedge a_1 > a_2 > 0\},$$
$$\mathcal{R'}_2 := \{a_1, a_2, d_1 \mid d_1 > 0 \wedge a_2 > a_1 > 0\}, \qquad (15)$$

but since we approach the boundary from two different directions, the two induced orientations are opposite (see appendix A for a detailed explanation). The region $\mathcal{R}'_1$ and $\mathcal{R}'_2$ share a codimension 1 boundary $(a_1 - a_2) = 0$ where the orientation changes sign. We call this an *internal boundary*.

We see that this boundary is in fact not oriented (rather it flips orientation on the internal boundary $a_1 = a_2$). Part of the definition of positive geometry in [10] is that it is oriented and, by the recursive nature of the definition, so are all boundaries etc. We conclude that a generalisation of the concept of positive geometry is needed to accommodate the loop amplituhedron.

Since both $\mathcal{R}'_1$ and $\mathcal{R}'_2$ by themselves *are* positive geometries on the other hand, their respective residues at $(a_2 - a_1) = 0$ are equal to the canonical form of this. Therefore the residue on the internal boundary of $\Omega(\mathcal{R}'_1) + \Omega(\mathcal{R}'_2)$ will be equal to twice the canonical form of a positive geometry. Note that if $\mathcal{R}'_1$ and $\mathcal{R}'_2$ instead had the same orientation as each other then $(a_2 - a_1) = 0$ would be a spurious boundary and the resulting residue would vanish.

We have thus seen that the loop amplitude has non-unit maximal residues and the geometrical origin of this is that the amplituhedron contains internal boundaries. In the next section we will see how to formalize what we have observed in this simple example and generalize the definition of the canonical form to geometries with internal boundaries, which will then accommodate the loop amplituhedron.

3 Generalized positive geometries and weighted positive geometries

3.1 Positive geometry and its canonical form

First we recall the definition of a positive geometry, $X_{\geq 0}$, and its canonical form, Ω, as defined recursively in [10], before we generalise this to accommodate internal boundaries. A positive geometry $X_{\geq 0}$ is an oriented region in some space (an algebraic variety) whose boundary consists of a set of positive geometries of one dimension less, with their orientation inherited from that of the neighbouring bulk geometry. Each component in this set lies inside some region of the form $f(x_i) = 0$ for some non-factorisable polynomial f. Then the associated canonical form, Ω, of $X_{\geq 0}$ is related to the associated canonical form, ω, of this boundary component via the residue form on $f(x_i) = 0$

$$df \wedge \operatorname{Res}_{f=0}\Omega = \lim_{f \to 0} f\Omega = df \wedge \omega. \qquad (16)$$

Since the dimension of the boundary component $f = 0$ is one dimension less than the dimension of X, this gives a recursive definition which stops when we reach dimension 0 positive geometries, which are just single points. These points are then defined to have canonical form ± 1 according to their orientation inherited from the original geometry. In the appendix A we review how the induced orientation is defined and the convention we use for the signs.

Apart from the 0-dimensional oriented points, the simplest examples of positive geometries are 1-dimensional. The most general 1d positive geometry is a disjoint union of intervals of arbitrary orientation. The canonical form of the interval from a to b is

$$[a,b] = \underset{a \qquad\qquad b}{\longrightarrow} \qquad\qquad \Omega([a,b]) = \frac{dx}{x-b} - \frac{dx}{x-a}. \tag{17}$$

The boundaries of this segment are given by $f(x) = x - b = 0$ and $f(x) = x - a = 0$, and we see from (16) that b has canonical form 1 and a has canonical form -1. The canonical form of the disjoint union of such intervals is simply the sum of the canonical forms of the intervals.

Notice that two intervals of the same orientation which share a common boundary point are equivalent to the larger interval

$$[a,b] \cup [b,c] = \underset{a \qquad\quad b \qquad\quad c}{\longrightarrow\longrightarrow} \quad = \quad \underset{a \qquad\qquad\qquad c}{\longrightarrow} \tag{18}$$

with the shared boundary point absent. This is reflected in the addition of the corresponding canonical forms

$$\Omega([a,b]) + \Omega([b,c]) = \Omega([a,c]). \tag{19}$$

In this case, the point b is sometimes called a spurious boundary.

However, two intervals of different orientations sharing a common boundary point

$$[a,b] \cup [c,b] = \underset{a \qquad\quad b \qquad\quad c}{\longrightarrow\longleftarrow} \tag{20}$$

does not constitute a positive geometry (for example, it is not oriented). Nevertheless, it is natural to associate to this geometry the corresponding canonical form

$$\Omega([a,b]) + \Omega([c,b]) = 2\frac{dx}{x-b} - \frac{dx}{x-a} - \frac{dx}{x-c}. \tag{21}$$

The point b is then special, separating two regions of opposite orientation, and we refer to this as an 'internal boundary'. It has residue twice that of each of the two individual boundaries there. This is exactly what we observed occurring for the two loop amplitude in the previous section.

3.2 Generalised positive geometry and its canonical form

The discussion above motivates a generalisation of the concept of positive geometry to incorporate internal boundaries. Internal boundaries separate two regions of opposite orientation. So, we define a generalised positive geometry as one whose internal and external boundaries are both generalised positive geometries. Both external and internal boundaries must lie inside a space defined by $f(x_i) = 0$ for some non-factorisable polynomial f. A particular subspace $f(x_i) = 0$ could contain both internal and external boundaries, each of which must be a (generalised) positive geometry with canonical form ω_{int} and ω_{ext} respectively. Then we define the canonical form recursively as

$$\text{Res}_{f=0}\Omega = \omega_{\text{ext}} + 2\omega_{\text{int}}, \tag{22}$$
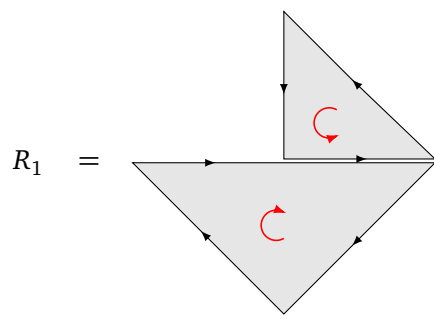
or equivalently,

$$\lim_{f \to 0} f\,\Omega \;=\; df \wedge (\omega_{\text{ext}} + 2\omega_{\text{int}})\,. \tag{23}$$

We see an extra term compared to the original canonical form for positive geometries (16), giving the factor of 2 associated with internal boundaries. The starting point for the recursion is the same as before; the 0-dimensional geometries, oriented points, with canonical form ± 1 according to their orientation. Note that the orientation of the interior boundary is unambiguously inherited from that of the bulk just as for the exterior boundaries.

So consider the 1d example in (20). This has external boundaries (with negative orientation) at $f_a(x) = x - a = 0$ and $f_c(x) = x - c = 0$ and an internal boundary with positive orientation at $f_b(x) = x - b = 0$. One can see that the canonical form (21) satisfies the recursive relation (22) at all three points.

Now consider a 2d example.

$$\tag{24}$$

Here the x axis contains both an external boundary and an internal boundary. The canonical form can be obtained straightforwardly by simply adding together the canonical forms of the two triangles,[4] giving

$$\Omega(R_1) = \frac{dx\,dy}{xy(x+y-1)} + \frac{2dx\,dy}{y(x+y+1)(x-y-1)}\,. \tag{25}$$

Now we can see how this satisfies the recursive definition (22) along the x axis. Taking the residue of (25) at $y = 0$ gives

$$\text{Res}_{y=0}\,\Omega = dx\left(\frac{1}{x} - \frac{1}{x+1}\right) + 2dx\left(\frac{1}{x-1} - \frac{1}{x}\right) = \Omega([-1,0]) + 2\Omega([0,1])\,, \tag{26}$$

which is exactly as predicted by (22) with $f = y$ since the external boundary on the x axis is the interval $[-1,0]$ and the internal boundary is $[0,1]$.

Note that internal boundaries give a contribution to the canonical form of twice that of a standard external boundary. One might think therefore that a leading singularity of any such a generalised positive geometry must be $0, \pm 1$ (as for a positive geometry) or ± 2 if there is an internal boundary present. However, there can be internal boundaries inside internal boundaries, leading to higher maximal residues. A very simple example of this is the region

---

[4]This key tessellation feature of positive geometries and the canonical forms is inherited by (and is indeed more powerful for) the generalised positive geometries as we will see.

consisting of the entire plane, but with the four quadrants having alternating orientations

$$R_2 \quad = \tag{27}$$

Here, each quadrant has exactly the same canonical form $dx\,dy/(xy)$ and so the geometry has non-zero canonical form

$$\Omega(R_2) = \frac{4dx\,dy}{xy}\,. \tag{28}$$

Taking the residue on the (internal) boundary $x = 0$ gives $\lim_{x\to 0}(x\Omega) = 2dx \wedge \left(\frac{2dy}{y}\right) = 2dx \wedge \omega_{int}$ with $\omega_{int} = \frac{2dy}{y}$, satisfying (22). Here the internal boundary in $x = 0$ is $(-\infty, 0)\cup(\infty, 0)$ and this itself has an internal boundary at $y = 0$. Thus it has canonical form $\frac{2dy}{y}$ (as we get directly from (21) by taking $b \to 0$, $a, c \to \infty$ and $x \to y$). So the leading singularity at $x = y = 0$ is 4.

It is also possible to get a leading singularity 3. Simply take three of the four quadrants from the previous example

$$R_3 \quad = \tag{29}$$

This geometry has canonical form

$$\Omega(R_2) = \frac{3dx\,dy}{xy}\,. \tag{30}$$

Here taking the residue on the boundary $x = 0$ gives $\lim_{x\to 0}(x\Omega) = dx \wedge \left(\frac{dy}{y}\right) + 2dx \wedge \left(\frac{dy}{y}\right)$ in agreement with (22). This time $x = 0$ contains the external boundary $(-\infty, 0)$ as well as the internal boundary $(0, \infty)$ both of which have canonical forms $\frac{dy}{y}$. Therefore, the leading singularity at $x = 0$ then $y = 0$ is 3.

Note that in [11], in the context of the squared amplituhedron, another generalisation of positive geometry was considered, and the associated canonical form called the globally oriented canonical form was defined. These geometries are in fact also examples of GPGs and we discuss this relation in more detail in appendix B.

3.3 Weighted positive geometry and its canonical form

Although the definition of the canonical form (22) is extremely compact, it has the downside of treating external and internal boundaries on a different footing. On the right hand side we

have a weighted sum of canonical forms, so it's tempting to rewrite this as the canonical form of a weighted sum of geometries. In this section we make this intuition precise by generalising what we mean by a geometrical region slightly, to include a weight taking arbitrary integer values. This articulates the idea of having multiple coinciding geometries which we naturally have when two regions meet on an internal boundary. This concept will allow us to give an explicit formula for maximal residues.

Firstly, recall that orientation on a space can be described by a top form where we are only really interested in the sign of the top form. So orientation is the equivalence class of real top forms modulo positive rescaling, $O \in \Omega^d / \sim$ where $O \sim \lambda O$ for any $\lambda > 0$. Now we extend this to define the weighted orientation as a pair $(w, O) : X \to (\mathbb{Z}, \Omega^d(X)) / \sim$ where here the equivalence relation involves positive or negative rescaling with the negative case also flipping the weight w

$$(w, O) \sim (\text{sign}(\lambda)w, \lambda O'), \qquad \lambda \neq 0. \tag{31}$$

Thus changing the orientation is equivalent to flipping the sign of w. In practise we can of course always choose coset representatives of (31) such that $w > 0$ and we will mostly assume this from now on.

Weighted geometries have a natural additive structure. At any point $x \in X$ we define the sum of two weighted geometries $(w_1, O_1) \oplus (w_2, O_2)$ as

$$(w_1, O_1) \oplus (w_2, O_2) = (w_1 + \text{sign}(\lambda)w_2, O_1), \tag{32}$$

where λ is such that $O_1 = \lambda O_2$.[5] Notice, that because of (31) this sum is symmetric and the identity element $(0, O)$ is unique.

So now we define a weighted geometry entirely by specifying its weight function and its orientation, rather than directly defining a region $X_\geq$. The region $X_\geq$ can be reconstructed by simply defining it as the set of points where $w \neq 0$. Boundaries are then places where the weighted orientation is discontinuous and they divide regions inside which the weighted orientation is continuous (and therefore w is constant). We will shortly define a canonical form for weighted geometries, the existence and uniqueness of which will define weighted positive geometries (WPG). For multivariate residues to be well defined, we insist that these boundaries must be subsets of algebraic varieties – so these regions are semi-algebraic sets.

A key aspect of this construction is that both weights and orientation on the boundaries are uniquely induced from those in the bulk. This happens as follows. Any boundary component, $\mathcal{C}$ can be defined through a polynomial $p(x) = 0$. Then one side of the boundary is $p(x) > 0$, with weight and orientation (w^+, O^+), whereas the other side is $p(x) < 0$ with (w^-, O^-). Now the region $p(x) > 0$ naturally induces the orientation $O^+|_{\mathcal{C}}$ on the boundary of the region $p > 0$ in the standard way (see appendix A), so $O^+ = dp \wedge O^+|_{\mathcal{C}}$. The region $p(x) < 0$ on the other hand naturally induces the orientation $O^-|_{\mathcal{C}}$ on the boundary, where $O^- = -dp \wedge O^-|_{\mathcal{C}}$.[6]

Given a codimension-1 variety $\mathcal{C} \in X$, then we define a projection operator $\Pi_{\mathcal{C}}$ that maps weighted orientations (w, O) on X to weighted orientations on $\mathcal{C}$ as

$$\Pi_{\mathcal{C}}(w, O) = (w^+|_{\mathcal{C}}, O^+|_{\mathcal{C}}) \oplus (w^-|_{\mathcal{C}}, O^-|_{\mathcal{C}}). \tag{33}$$

Choosing representatives such that $w > 0$, we can give the following two dimensional illustra-

---

[5] Note that the x dependence is suppressed in the equation and that the function $\text{sign}(\lambda(x))$ is negative if the two orientations $O_1(x)$ and $O_2(x)$ are opposite and positive if they match.

[6] The minus sign arises from the fact that the normal vector pointing inward the region $p < 0$ is $-\partial_p$.

tion of the induced weights and orientations (denoted with arrows):

$$\tag{34}$$

Note that w or w' could have been zero in which case we have a conventional external boundary. This definition implies that, for $w(x) = 1$ in $X_{>0}$ and 0 otherwise, $w|_{\mathcal{C}}$ will be equal to 2 on internal boundaries, to 1 on external boundaries and 0 otherwise. In this formulation internal and external boundaries are not distinguished. Furthermore note that if $w^+ = w^-$ and $\lambda < 0$ then there are equivalent weighted orientations on both sides (meaning the induced orientations are opposite) and thus there is no genuine boundary there (it is a spurious boundary).

An important observation now is that the projection Π is a linear operator

$$\Pi_{\mathcal{C}}\Big((w_1, O_1) \oplus (w_2, O_2)\Big) = \Pi_{\mathcal{C}}(w_1, O_1) \oplus \Pi_{\mathcal{C}}(w_2, O_2), \tag{35}$$

which can be easily proven from the definitions.

Now we can define a weighted positive geometry as a weighted geometry possessing a canonical form. The definition of the canonical form of a weighted geometry is defined recursively such that the residue of the canonical form on $\mathcal{C}$ is the canonical form of the geometry projected on $\mathcal{C}$:

$$\operatorname{Res}_{\mathcal{C}} \Omega(w, O) = \Omega(\Pi_{\mathcal{C}}(w, O)). \tag{36}$$

The recursion starts by defining the canonical form of a zero dimensional weighted geometry (for which O is a 0 form, simply a scalar) as the product of w with the sign of O

$$\Omega(w, O) = w \operatorname{sign}(O) \qquad (\text{In zero dimensions}). \tag{37}$$

In zero dimensions therefore the canonical form is a linear operator

$$\Omega\Big((w_1, O_1) \oplus (w_2, O_2)\Big) = \Omega\Big(w_1 + \operatorname{sign}(\lambda) w_2, O_1\Big) = (w_1 + \operatorname{sign}(\lambda) w_2) \times \operatorname{sign}(O_1)$$
$$= w_1 \operatorname{sign}(O_1) + w_2 \operatorname{sign}(O_2) = \Omega(w_1, O_1) + \Omega(w_2, O_2), \tag{38}$$

where recall $O_1 = \lambda O_2$. It follows by induction from the recursive definition (36) and linearity of the projection operator Π (35) that this linearity property of Ω then holds for spaces of arbitrary dimension:

$$\Omega\Big((w_1, O_1) \oplus (w_2, O_2)\Big) = \Omega(w_1, O_1) + \Omega(w_2, O_2). \tag{39}$$

Remarkably we have the feature that we can freely sum arbitrary (even overlapping) WPGs! It also follows directly from this that

$$\Omega\Big((\lambda w, O)\Big) = \lambda \Omega(w, O). \tag{40}$$

Now given a sequence of boundaries $\{\mathcal{C}_1, \cdots, \mathcal{C}_n\}$, we can follow n steps of the recursion (36) and write the multi-residue of a canonical form as the canonical form of the multiply induced boundary

$$\operatorname{Res}_{\mathcal{C}_1, \cdots, \mathcal{C}_n} \Omega(w, O) = \Omega(\Pi_{\mathcal{C}_1, \cdots, \mathcal{C}_n}(w, O)). \tag{41}$$

Then taking $n = d$, the dimension of X, we obtain an expression for the maximal residues in terms of the canonical form at a point (37)

$$\text{Res}_{\mathcal{C}_1,\cdots,\mathcal{C}_d}\Omega(w,O) = w_{\mathcal{C}_1,\cdots,\mathcal{C}_d} \times \text{sign}\left(O_{\mathcal{C}_1,\cdots,\mathcal{C}_d}\right), \tag{42}$$

where $(w_{\mathcal{C}_1,\cdots,\mathcal{C}_d}, O_{\mathcal{C}_1,\cdots,\mathcal{C}_d}) = \Pi_{\mathcal{C}_1,\cdots,\mathcal{C}_d}(w,O)$. This last equation can also be used as a direct, non-recursive, definition of the canonical form by giving all its maximal residues (the canonical form is completely determined by its maximal residues).

Note that generalised positive geometries, defined in previous subsections, should simply be WPGs for which the weight function (in the bulk) is $w = \pm 1, 0$ everywhere. Similarly positive geometries are WPGs for which the weight function $w = \pm 1, 0$ everywhere (so they are also GPGs) but also the induced weight function on all nested boundary components is also always $\pm 1, 0$.

To check this we need to show that the canonical form for the GPGs defined by (22) and that for the WPGs (36) are equivalent. By equivalent we mean that given any GPG $X_{\geq 0}$ with orientation O we associate a weighted geometry with orientation O and weight w such that $w(x) = 1$ for all $x \in X_{\geq 0}$ and zero otherwise, and then

$$\Omega(X_{\geq 0}) = \Omega(w,O). \tag{43}$$

Now notice that the projection of (w, O) onto $\mathcal{C}$ (described in (33) and above) will have induced weight 1 or 2, depending on whether it is an external or internal boundary. So we can write $\Pi_{\mathcal{C}}(w,O) = (w_{\text{ext}}, O_{\text{ext}}) \oplus (w_{\text{int}}, O_{\text{int}})$ where $w_{\text{ext}} = 1$ on external boundaries and zero elsewhere whereas $w_{\text{int}} = 2$ on internal boundaries and zero elsewhere. Then, it follows that if we apply (36) we get

$$\text{Res}_{\mathcal{C}}\Omega(w,O) = \Omega\left(\Pi_{\mathcal{C}}(w,O)\right) = \Omega((w_{\text{ext}}, O_{\text{ext}}) \oplus (w_{\text{int}}, O_{\text{int}})) = \Omega(w_{\text{ext}}, O_{\text{ext}}) + 2\Omega\left(\frac{w_{\text{int}}}{2}, O_{\text{int}}\right). \tag{44}$$

Now since w_{ext} and $\frac{1}{2}w_{\text{int}}$ are both functions respectively equal to 1 on internal and external boundaries and equal to 0 otherwise, they represent with their orientations the external and internal boundaries as GPGs. This is then precisely the original defining equation of the canonical form (22). Since we showed that the recursion (36) and (22) have the same form it follows that the two definitions of the canonical form give the same result.

Finally, let us illustrate with a slightly more involved example, returning to the case considered in (29) from this new perspective

$$\tag{45}$$

Here we see the induced weights 2,1 on the codimension 1 boundaries $x = 0, y = 0$. Considering these boundaries themselves they then induce the weight $2 + 1 = 3$ at the origin with positive orientation on the y axis, negative on the x axis. This is in line with (42) and the corresponding maximal residue $\text{Res}_{y=0,x=0}\Omega_{R_3} = -\text{Res}_{x=0,y=0}\Omega_{R_3} = 3$.

Note that in [10] a generalisation of positive geometries was defined, the Grothendieck group of pseudo-positive geometries, consisting of the formal sum of positive geometries modded out by geometries with vanishing canonical form. The Grothendieck group of pseudo-positive geometries and the WPGs are closely related but different. The Grothendieck group

of pseudo-positive geometries is presumably equivalent to the space of WPGs after modding out by elements with zero canonical form. This equivalence relation implies that

$$\Omega((w_1, O_1)) = \Omega((w_2, O_2)) \quad \Rightarrow \quad (w_1, O_1) \sim (w_2, O_2). \tag{46}$$
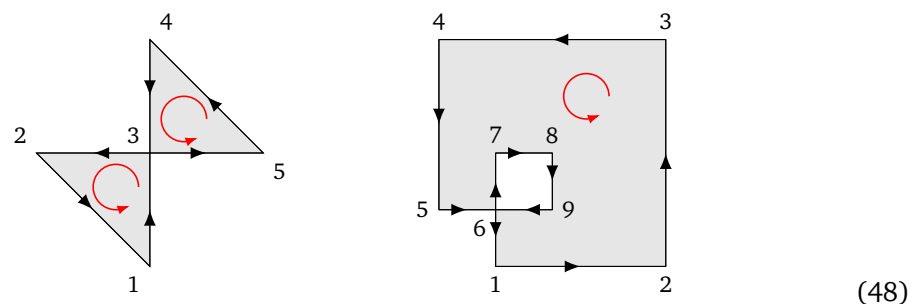
3.4 Uniqueness of the canonical form

The uniqueness of the canonical form for GPG/WPGs is equivalent to the statement that the algebraic variety on which the positive geometry lives has geometric genus zero ie has no non-zero holomorphic volume forms, just as for PGs [10]. Since holomorphic forms have no poles, they could be added to any canonical form to obtain a new canonical form satisfying all the requirements and thus we would not have a unique canonical form. Conversely, under the assumption that GPGs/WPGs have no holomorphic forms, we can proceed by induction assuming that the canonical form in $d-1$ dimensions is always unique. Consider two canonical forms Ω_1, Ω_2 for the same GPG or WPG. By definition, both forms have poles only on the boundary components. The residue on a boundary component is the canonical form of the boundary component, by the recursive definition of the canonical form. But since by induction we assumed that the canonical form in $d-1$ dimensions is unique then we conclude that for any residue $\text{Res}(\Omega_1 - \Omega_2) = 0$, and so $\Omega_1 - \Omega_2$ has no poles and is thus a holomorphic form and so must vanish. We conclude that $\Omega_1 = \Omega_2$ and so the canonical form is unique.

3.5 Tilings

A fundamental property of the canonical form is that given a positive geometry $X_{\geq 0}$ and a set of positive geometries $X_{\geq 0}^{(i)}$ tiling $X_{\geq 0}$,[7] then the canonical form of $X_{\geq 0}$ is the sum of that of the tiles

$$\Omega(X_{\geq 0}) = \sum_i \Omega\left(X_{\geq 0}^{(i)}\right). \tag{47}$$

However it can happen that a non positive geometry can be triangulated by positive geometries - so the space of positive geometries is not closed under the union. This is because even if the orientation of the $X_{\geq 0}^{(i)}$ tiling $X_{\geq 0}$ matches on codimension 1 boundaries this does not imply that they will necessarily match on the boundaries of boundaries etc. This can then give rise to internal boundaries. As examples consider the following two geometries:

$$\tag{48}$$

Both can be triangulated by positive geometries. The first can be triangulated as the oriented union of two triangles while the second as the oriented union of 4 rectangles with matching orientation. Both examples are not positive geometries themselves however. This can be seen graphically observing the orientation of the boundary, the edge 14 in the first example and 59 in the second look like (20) and have an internal boundary.

---

[7]By a tiling we mean the $X_{\geq 0}^{(i)}$ cover $X_{\geq 0}$ with non-overlapping regions. We will often also call such a tiling a triangulation.

Both of these examples *are* generalised positive geometries however. And we claim more generally that if $X_{\geq 0}$ is triangulated by a set of generalized positive geometries $X_{\geq 0}^{(i)}$ tiling $X_{\geq 0}$ then $X_{\geq 0}$ is a generalized positive geometry and its canonical form is given by (47). Thus the space of GPGs is closed under the disjoint-union. This is essentially trivial from linearity of the WPG canonical form and the definition of a GPG as a WPG with weight $0, \pm 1$ everywhere.

A beautiful consequence of the WPG formalism is that it also yields a simple proof of the tiling property of positive geometries (47). Indeed this follows trivially from the fact that the canonical form is a linear operator for weighted positive geometries (39). Translating (47) into WPG language, on the right hand side we have the canonical form of a region which is equivalently a weight function (w, O) with $w = 1$ in the region and 0 outside. This region has a tesellation with tiles (w_i, O_i) with

$$(w, O) = \bigoplus_i (w_i, O_i). \tag{49}$$

Now linearity of WPGs give

$$\Omega(w, O) = \sum_i \Omega(w_i, O_i), \tag{50}$$

which proves (47).

3.6 Speculations on an explicit characterisation of GPGs / WPGs

In the previous subsection we gave an implicit (recursive) definition of generalised positive geometry and weighted positive geometries. Here we consider whether it is possible to give more explicit characterisations, so we can know in advance if a particular region is a GPG/WPG or not. The fact that GPGs/WPGs are closed under union (or sum for WPGs) as discussed in the previous subsection already suggests they ought to be more amenable to a direct characterisation than PGs. For example any characterisation of PGs would have to exclude the two examples in (48).

We first note that if we restrict ourselves to a specific class of geometry which we call *multi-linear geometries* then the characterisation is very simple. Multi-linear geometries are geometries defined by *multi-linear inequalities* in some coordinates. Note that although this may be a big restriction of the full space of positive geometries it nevertheless provides a very wide class of cases. Crucially it is straightforward to see that the amplituhedron is a multi-linear geometry. The defining inequalities of the amplituhedron are given in terms of either minors of a C matrix, or alternatively determinants of the form $\langle Y L_i ... \rangle$. Thus by choosing components of either the C matrix, and/or the Y, L_i as coordinates, the resulting inequalities will be multi-linear in those coordinates (simply because the determinant is a multi-linear function of its components).

Note here that it is important not to confuse multi-linear geometries with linear geometries. Many of the toy examples one considers are linear geometries where defining inequalities can be given which are linear in all variables. These then have straight edges, flat planes etc. Multi-linear geometries can however be curvey. For example in 2d, boundaries of multi-linear geometries have the form $axy + bx + cy + d = 0$ (in some coordinates) which correspond to hyperbolas as well as straight lines. On the other hand circles or ellipses would include the non multi-linear terms x^2, y^2 and are not multi-linear. They can however be boundaries of positive geometries [10]. We will shortly return to this point.

We first claim that *any* multi-linear geometry is a (generalised) positive geometry. We can show this by explicitly and uniquely computing the canonical form for multi-linear geometries. Given a multi-linear geometry, first use cylindrical decomposition (see also [20]) which recasts

any region as a disjoint union of regions $\mathcal{R}_i$ of the form

$$
\mathcal{R}_i := \{x_1, \cdots, x_d\}, \quad \text{st} \quad
\begin{cases}
\quad\quad\quad a_1 < x_1 < b_1, \\
\quad\quad a_2(x_1) < x_2 < b_2(x_1), \\
\quad\quad\quad\quad \cdots, \\
a_d(x_1, \cdots, x_{d-1}) < x_d < b_d(x_1, \cdots, x_{d-1}),
\end{cases}
\tag{51}
$$

for some functions a_j, b_j. Now changing variables to:

$$
x'_j = -\frac{x_j - a_j}{x_j - b_j},
\tag{52}
$$

then $\mathcal{R}_i$ becomes

$$
\mathcal{R}_i := \{x'_1, \cdots, x'_d\}, \quad \text{st} \quad x'_j > 0, \quad \text{for all } j.
\tag{53}
$$

In the new coordinates $\mathcal{R}_i$ is thus a simplex-like positive geometry with canonical form

$$
\Omega(\mathcal{R}_i) = \prod_{j=1}^{d} \frac{d x'_j}{x'_j}.
\tag{54}
$$

But as discussed in [10] under a *rational* map the canonical forms map to each other. So as long as the change of variables (52) is rational then we have that in the original coordinates

$$
\Omega(\mathcal{R}_i) = \prod_{j=1}^{d} \left(\frac{1}{x_j - a_j} - \frac{1}{x_j - b_j} \right) d x_j,
\tag{55}
$$

and the canonical form of the full region can then be obtained by summing the contributions from all the $\mathcal{R}_i$. We see how multi-linearity is crucial here. The inequalities in (51) must arise from the defining inequalities of our region which are multi-linear. This ensures that the resulting functions a_i and b_i will be rational functions and thus the change of variables (52) is rational.

Let us illustrate some of these points now with a couple of examples shown in figure 1.

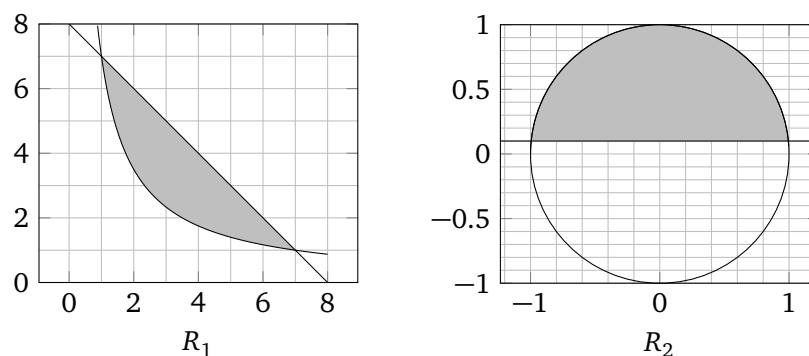Figure 1: Two examples of positive geometries obtained by sandwiching a conic and a straight line. The first, involving a hyperbola, is a multi-linear geometry whereas the second is not multi-linear, but is still a positive geometry.

Firstly we have a region R_1 sandwiched between a hyperbola and a line. It is defined by the inequalities $x > 0, xy > 7, x + y < 8$. Cylindrical decomposition rewrites this as a single

region written in the form of (51) as $1 < x < 7 \quad \frac{7}{x} < y < 8 - x$. Then the simple replacement rule of (55) yields the canonical form

$$\Omega(R_1) = \left(\frac{dx}{x-1} - \frac{dx}{x-7} \right) \left(\frac{dy}{y - \frac{7}{x}} - \frac{dy}{x+y-8} \right) = -\frac{6\,dx\,dy}{(x+y-8)(xy-7)}. \tag{56}$$

The second example R_2, found in [10], is not a multi-linear geometry. This is the region between a circle and a line and is defined by the inequalities $x^2 + y^2 < 1, y > 1/10$. Let us see what happens if we attempt the same procedure to obtain its canonical form. Here cylindrical decomposition rewrites the region as

$$-\frac{3\sqrt{11}}{10} < x < \frac{3\sqrt{11}}{10}, \qquad \frac{1}{10} < y < \sqrt{1-x^2}. \tag{57}$$

But now we encounter a problem. We see that, due to the square root $\sqrt{1-x^2}$, the change of variables needed in (52) will no longer be rational and the above procedure no longer works.

So we have seen that cylindrical decomposition gives the unique canonical form as long as all the resulting functions a_i, b_i in (51) are rational. This is clearly the case for multi-linear geometries, but could also be the case for more general geometries. Further it may be possible to change coordinates so that only in the new coordinates the cylindrical decomposition map (52) is rational. So in general we can characterise generalised positive geometries to be those for which there exist coordinates and an ordering of these coordinates such that cylindrical decomposition yields a map (52) which is rational.

For example let us return to the region R_2 in figure 1 for which the cylindrical decomposition method of obtaining the canonical form didn't work as it produces an irrational map (52). Now the circle is the classic example of a rational variety. This is a variety that has a parametrisation t_i in terms of which its embedding coordinates $x_i(t_j)$ are rational functions and there is a rational inverse map $t_i(x_j)$. In this case it has a rational parametrisation given by

$$x(t) = \frac{2t}{1+t^2}, \qquad y(t) = \frac{1-t^2}{1+t^2}, \tag{58}$$

with an inverse map from $\mathbb{R}$ onto the circle embedded in $\mathbb{R}^2$ which is also rational

$$t(x,y) = \frac{x}{1+y}. \tag{59}$$

Here the parameter t has the geometrical interpretation of the projection of a point on the circle, from the point $(0,-1)$ to the x axis. But this projection can clearly be extended to any point in $\mathbb{R}^2$ not just those points on the circle. So consider the change of variables from x to t, $(t,y) \to (x,y) = (t(1+y),y)$. In the new variables the region R_2 then has cylindrical decomposition

$$-\frac{3}{\sqrt{11}} < t < \frac{3}{\sqrt{11}}, \quad \frac{1}{10} < y < \frac{1-t^2}{t^2+1}, \tag{60}$$

which is now rational. The replacement rule (55), then gives the canonical form

$$\Omega(R_2) = -\frac{6\sqrt{11}dt\,dy}{(10y-1)(t^2(y+1)+y-1)} = -\frac{6\sqrt{11}dxdy}{(10y-1)(x^2+y^2-1)}, \tag{61}$$

which is in precise agreement with the canonical form for this geometry found in [10] (see figure 1) using the recursive definition of the canonical form.

In general, if a codimension 1 boundary of a region is a rational variety, then changing coordinates from x_i to t_i, x_n will rationalise the final step in the cylindrical decomposition involving that boundary. In other words cylindrical decomposition in those variables will give the boundary in the form $x_n < x_n(t_i)$ which is a rational function as we saw in the above example which gave $y < y(t) = (1-t^2)/(1+t^2)$). This all suggests there should be a more intrinsic definition of a GPG/WPG in terms of rational varieties.

4 All-in-one-point cut

We now look at a particular boundary of the loop amplituhedron related to a set of cuts on the integrand of MHV amplitudes explored in [18, 21], referred to as the *deepest cut*. This provides another example of an internal boundary as well as illustrating the other important point mentioned in the introduction, namely that the order of taking residues (or going to boundaries) can yield completely different results.

In general the deepest cut places all internal propagators on-shell

$$\langle (AB)_\alpha (AB)_\beta \rangle = 0, \quad \forall \ \alpha, \beta = 1, ..., l, \tag{62}$$

while leaving all external propagators $\langle (AB)_\alpha ii+1 \rangle$ generic. Geometrically there are two possible final configurations which solve (62): first, all loop lines passing through a single point A, or second, all loop lines lying on the same plane. In [18] the canonical form corresponding to these two solutions was found at any loop order. We find that this form can not be reproduced from any sequence of single residues (or any linear combination of such) acting on the amplitude and so some more complicated operation is presumably needed to reproduce it.[8] Furthermore there are many inequivalent ways of approaching this final all-in-one-point configuration via different sequences of single residues, as becomes especially apparent starting at four loops. In this section we systematically investigate all cuts ending in the all-in-one-point configuration.

We will begin by discussing the three loop all-in-one-point cut, computing its geometry and discussing the internal boundary that arises, before considering higher loops. Although we will limit the discussion to the 4-point MHV amplituhedron geometry, the derivation of the geometry is completely independent of the tree level inequalities $\langle Yijkl \rangle$ and $\langle ABij \rangle$. The results obtained in section 4.3 for the loop-loop inequalities of the all-in-one-point cut hold for any multiplicity and any NMHV degree by simply promoting the brackets $\langle AB_iB_jB_k \rangle$ to $\langle YAB_iB_jB_k \rangle$.

4.1 Three-loop all-in-one-point cut

The first case of an all-in-one-point cut is at two loops. Although we saw above that this contains a previously undetected internal boundary, since the all-in-one-point cut *is* this boundary it doesn't affect anything and the corresponding residue is simply the canonical form of two lines satisfying 1 loop inequalities as predicted in [18]. We will return to this in section 5.1.

We thus turn to three loops. The integrand of the three-loop MHV amplitude is given by

$$\text{MHV}(3) = \frac{\prod_{i=1}^3 \langle A_iB_i d^2A_i \rangle \langle A_iB_i d^2B_i \rangle \langle 1234 \rangle^3}{\langle A_1B_114 \rangle \langle A_1B_112 \rangle \langle A_1B_134 \rangle \langle A_2B_212 \rangle \langle A_2B_223 \rangle \langle A_3B_334 \rangle \langle A_1B_1A_3B_3 \rangle \langle A_2B_2A_3B_3 \rangle}$$
$$\times \left[\frac{1}{2} \frac{\langle 1234 \rangle}{\langle A_3B_312 \rangle \langle A_2B_234 \rangle} + \frac{\langle A_1B_123 \rangle}{\langle A_3B_323 \rangle \langle A_1B_1A_2B_2 \rangle} \right] + \text{ symmetry}. \tag{63}$$

---

[8]We thank Nima Arkani-Hamed and Jaroslav Trnka for valuable discussions on this point.
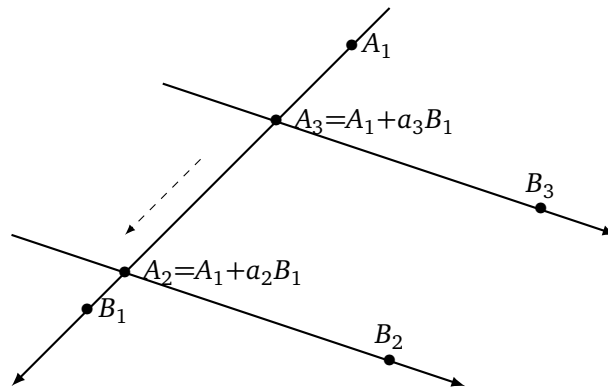
Figure 2: A geometrical depiction of the third residue taken when calculating the three loop all-in-one-point cut. Note the lines that pass through the points B_2 and B_3 do not in general lie on the same plane, but they do not (yet) intersect.

Here the '+ symmetry' is a sum of 23 more terms: the 3! terms generated by permutation symmetry over the loop variables (simultaneous permutation of A_i and B_i) together with the four terms from cyclic symmetry of the external twistors, giving 24 terms in total in the sum. The first term in square brackets is the three-loop ladder integrand, and after summing it generates 12 unique terms (all with coefficient 1), while the second term is the so-called 3-loop 'tennis court' diagram generating 24 unique terms (again all will have coefficient 1).

In order to achieve an all-in-one-point final configuration – with three loop lines passing through a single point A – we must take three residues at $\langle A_i B_i A_j B_j \rangle = 0$ (62). By inspection, one can see that the first term in square brackets in (63) (the ladder integral) does not contain all three poles $\langle A_i B_i A_j B_j \rangle$ and therefore vanishes after taking these residues. From this point forward then we will only concern ourselves with the second term.

The key factor which all surviving terms contain is

$$F = \frac{\prod_{i=1}^{3} \langle A_i B_i \mathrm{d}^2 A_i \rangle \langle A_i B_i \mathrm{d}^2 B_i \rangle}{\langle A_1 B_1 A_2 B_2 \rangle \langle A_2 B_2 A_3 B_3 \rangle \langle A_1 B_1 A_3 B_3 \rangle}. \tag{64}$$

We will then first consider the residue at $\langle A_1 B_1 A_2 B_2 \rangle = 0$ followed by $\langle A_1 B_1 A_3 B_3 \rangle = 0$. This corresponds geometrically to first intersecting the line $A_2 B_2$ with $A_1 B_1$ and then $A_3 B_3$ with $A_1 B_1$ (see 2). To do this, we parametrise A_2 and A_3 as

$$\begin{aligned} A_2 &= A_1 + a_2 B_1 + b_2 Z_*, \\ A_3 &= A_1 + a_3 B_1 + b_3 Z_*, \end{aligned} \tag{65}$$

where Z_* is an arbitrary twistor. In this parametrisation, the limits $b_2 \to 0$ and $b_3 \to 0$ correspond to the points A_2 and A_3 moving to lie on the line $A_1 B_1$ respectively. Using this parametrization, we have for example that $\langle A_2 B_2 \mathrm{d}^2 A_2 \rangle = \mathrm{d}b_2 \mathrm{d}a_2 \langle A_1 B_2 Z_* B_1 \rangle$ etc. and the factor (64) produces $\mathrm{d}b_2 \mathrm{d}b_3 / (b_2 b_3)$. Taking the residue then gives

$$\operatorname*{Res}_{\substack{\langle A_1 B_1 A_2 B_2 \rangle = 0 \\ \langle A_1 B_1 A_3 B_3 \rangle = 0}} F = \frac{\mathrm{d}a_2 \mathrm{d}a_3 \langle A_1 B_1 \mathrm{d}^2 A_1 \rangle \prod_{i=1}^{3} \langle A_i B_i \mathrm{d}^2 B_i \rangle}{\langle A_2 B_2 A_3 B_3 \rangle}. \tag{66}$$

With the parametrisations (65), with $b_2 = b_3 = 0$ we see that the remaining singularity of F factorises into two terms $\langle A_2 B_2 A_3 B_3 \rangle = (a_2 - a_3) \langle A_1 B_1 B_2 B_3 \rangle$. This is another example of composite residues discussed in the introduction and section 2. The first factor $a_2 - a_3 = 0$ corresponds to the three loop lines intersecting in one point, while $\langle A_1 B_1 B_2 B_3 \rangle = 0$ corresponds

to the three lines lying in the same plane (and thus intersecting pairwise). We focus on the all-in-one-point case $(a_2-a_3) \to 0$ (intersecting A_3B_3 with A_2B_2 by sliding the intersection point A_3 along the line A_1B_1 to meet the intersection point A_2 see figure 2). We change variables from (a_2, a_3) to (a_2, ξ) where $\xi = (a_2-a_3)$, so $da_2 da_3 = d\xi da_2$ and the residue at $\xi \to 0$ of (66) is

$$\underset{\xi=0}{\text{Res}} \left(\frac{d\xi da_2}{\xi} \frac{\langle A_1 B_1 d^2 A_1 \rangle \prod_{i=1}^{3} \langle A_i B_i d^2 B_i \rangle}{\langle A_1 B_1 B_2 B_3 \rangle} \right) = \frac{\langle A d^3 A \rangle \prod_{i=1}^{3} \langle A B_i d^2 B_i \rangle}{\langle A B_1 B_2 B_3 \rangle} \,. \qquad (67)$$

On the right-hand side we have written the expression manifestly as a function of the common intersection point of all three lines $A = A_1 + a_2 B_1$, thus $da_2 \langle A_1 B_1 d^2 A_1 \rangle = \langle A d^3 A \rangle$.

Substituting (67) into (63) gives the all-in-one-point cut of the three loop amplitude :

$$\frac{\langle A d^3 A \rangle \prod_{i=1}^{3} \langle A B_i d^2 B_i \rangle}{\langle A B_1 B_2 B_3 \rangle} \left(\frac{\langle 1234 \rangle^3 \langle A B_1 23 \rangle}{\langle A B_1 14 \rangle \langle A B_1 12 \rangle \langle A B_1 34 \rangle \langle A B_2 12 \rangle \langle A B_2 23 \rangle \langle A B_3 23 \rangle \langle A B_3 34 \rangle} + \text{symmetry} \right),$$
$$(68)$$

where the sum occurs by applying cyclic symmetry of the external momenta and permutation symmetry of the B_is. We see that after taking the three consecutive residues required to reach this final configuration, a new pole $\langle A B_1 B_2 B_3 \rangle$ appears explicitly in the denominator of the integrand. This is not the same as the result given for the all-in-one-point cut in [18] which is instead the canonical form of the intersection of the hyperplane $\langle A_i B_i A_j B_j \rangle = 0$ with the amplituhedron.[9] Taking further residues of this all-in-one-point cut, starting with the pole $\langle A B_1 B_2 B_3 \rangle$ one ends up with a maximal residue of 2 (see appendix C for this computation) which, as discussed in section 2 suggests the existence an internal boundary.

In the next subsection we therefore look at the geometrical region corresponding to taking the above all-in-one-point cut. We will find that the pole at $\langle A B_1 B_2 B_3 \rangle = 0$ indeed corresponds geometrically to an internal boundary of the codimension 3 boundary of the four-point three-loop amplituhedron corresponding to the all-in-one-point cut.

4.2 Geometric all-in-one-point cut

We now look to derive the geometry of the all-in-one-point cut. Following precisely the residues taken in section 4.1, we first intersect line L_1 with L_2, then intersect L_3 with L_1, and finally intersect L_2 and L_3 by sliding A_3 along L_1.

The four-point loop level amplituhedron is defined as the set of loop lines $L_i = (A_i B_i)$ with $i = 1, .., L$ satisfying

$$\mathcal{A}^{(L)} = \left\{ A_i B_i : \langle A_i B_i \bar{k} \bar{l} \rangle > 0, \ \langle A_i B_i A_j B_j \rangle > 0, \quad 1 \leq i, j \leq L, \ 1 \leq k < l \leq 4 \right\}. \qquad (69)$$

Here for each loop we have the inequalities of the one loop amplituhedron

$$\begin{aligned} \langle A_i B_i 12 \rangle > 0, \quad \langle A_i B_i 13 \rangle < 0, \quad \langle A_i B_i 14 \rangle > 0, \\ \langle A_i B_i 23 \rangle > 0, \quad \langle A_i B_i 24 \rangle < 0, \quad \langle A_i B_i 34 \rangle > 0, \end{aligned} \qquad (70)$$

which can all be conveniently rewritten in terms of the conjugate planes as [18]

$$\langle A_i B_i \bar{j} \bar{k} \rangle > 0, \qquad 1 \leq j < k \leq 4, \qquad (71)$$

---

[9]Note that if one instead takes an antisymmetric sum over the B_i permutations in (68), the result produces a zero in $\langle A B_1 B_2 B_3 \rangle$, cancelling the pole and reproducing the deepest cut given in [18]. We can not obtain this via an operation acting on the amplitude however but rather one would have to take a different operation on each contributing diagram.

where $\bar{j} \equiv (j-1jj+1)$ and $\langle A_i B_i \bar{j}\bar{k}\rangle \equiv \langle A_i B_i (j-1jj+1) \cap (k-1kk+1)\rangle$. We then also have the loop-loop inequalities, $\langle A_i B_i A_j B_j\rangle > 0$. The all-in-one point configuration occurs when all loop lines L_i pass through a single point A, so we simply set $A_i = A$. Then the loop-loop inequalities trivialise and this all-in-one-point cut geometry is

$$\mathcal{A}_{dc}^{(L)} = \mathcal{A}^{(L)}|_{A_i=A} = \left\{ A, B_i : \langle AB_i \bar{k}\bar{l}\rangle > 0, \ \ 1 \le k < l \le 4 \right\}. \tag{72}$$

This is the codimension 3 configuration of the amplituhedron corresponding to all loop lines intersecting in one point.
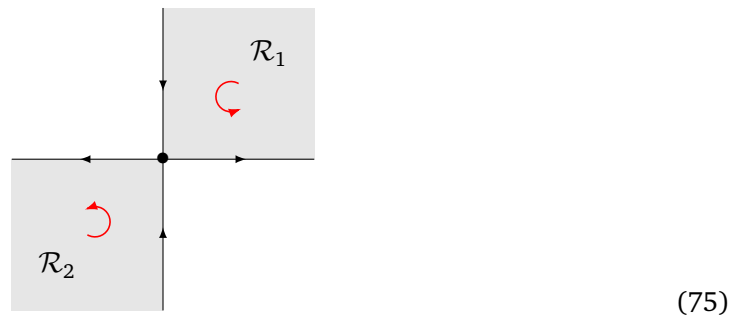
We now however wish to examine in detail what happens when we take a sequence of codimension 1 boundaries in order to reach such a configuration. Using the same parametrisation as (65), $A_2 = A_1 + a_2 B_1 + b_2 Z_*$, $A_3 = A_1 + a_3 B_1 + b_3 Z_*$ the loop-loop inequalities become

$$
\begin{aligned}
\langle A_1 B_1 A_2 B_2\rangle &= -b_2 \langle A_1 B_1 B_2 Z^*\rangle > 0, \\
\langle A_1 B_1 A_3 B_3\rangle &= b_3 \langle A_1 B_1 Z^* B_3\rangle > 0, \\
\langle A_2 B_2 A_3 B_3\rangle &= (a_2 - a_3)\langle A_1 B_1 B_2 B_3\rangle + (b_2 - b_3)\langle A_1 Z_* B_2 B_3\rangle > 0.
\end{aligned}
\tag{73}
$$

We then consider the boundary at $a_2 = a_3$ of the boundary at $b_3 = 0$ of the boundary at $b_2 = 0$, which corresponds precisely to taking the consecutive residues of (66) and below. Here Z_* is chosen arbitrarily and we can arrange it so that $\langle A_1 B_1 B_2 Z_*\rangle < 0$ and $\langle A_1 B_1 Z_* B_3\rangle > 0$ and thus $b_2, b_3 > 0$. Notice that the third inequality factorises when $b_2, b_3 \to 0$. This is the geometric version of the factorisation discussed below (66), related to composite residues and reducible varieties. Thus the boundary at $b_2, b_3 \to 0$ is the union of two disconnected regions $\mathcal{R}_1 \cup \mathcal{R}_2$

$$
\begin{aligned}
\mathcal{R}_1 : & \quad a_2 > a_3, \quad \langle AB_1 B_2 B_3\rangle > 0, \\
\mathcal{R}_2 : & \quad a_2 < a_3, \quad \langle AB_1 B_2 B_3\rangle < 0,
\end{aligned}
\tag{74}
$$

where $A = A_1 + a_2 B_1$. The inequalities, (74), carve out a region consisting of two almost disconnected pieces of the same orientation. This geometry is illustrated in the picture (the same as for the two-loop internal boundary case (12))

$$\tag{75}$$

where the x axis corresponds to the region $a_2 = a_3$ and the y axis corresponds to $\langle AB_1 B_2 B_3\rangle = 0$. The all-in-one-point cut corresponds to the boundary $a_2 = a_3$ (so the x axis). We can then clearly see that the all-in-one-point cut consists of two regions, $\langle AB_1 B_2 B_3\rangle \lessgtr 0$, with opposite orientation separated by an (internal) boundary at $\langle AB_1 B_2 B_3\rangle = 0$:

$$\langle AB_1 B_2 B_3\rangle < 0 \qquad\qquad \langle AB_1 B_2 B_3\rangle > 0$$

$$\tag{76}$$

Geometrically the two regions arise from the intersection point A_3 approaching A_2 from two different directions along the line $A_1 B_1$ (see figure 2). Importantly, after approaching the all-in-one-point cut, the mutual positivity conditions between the loops of (73) do not trivialise, but instead new inequalities emerge dictated by the sign of $\langle AB_1 B_2 B_3\rangle$.

So altogether then, incorporating the inequalities resulting from (70) (rewritten as in (71)) we see that the the full geometry of the three-loop all-in-one-point cut is given by the two regions with opposite orientation

$$
\begin{aligned}
\mathcal{R}^{dc} &= \mathcal{R}_1^{dc} \cup \mathcal{R}_2^{dc}, \\
\mathcal{R}_1^{dc} &= \mathcal{A}_{dc}^{(3)} \cap \{\langle AB_1B_2B_3 \rangle > 0\}, & \text{positive orientation}, \\
\mathcal{R}_2^{dc} &= \mathcal{A}_{dc}^{(3)} \cap \left\{\langle AB_1B_2B_3 \rangle < 0\right\}, & \text{negative orientation}.
\end{aligned}
\tag{77}
$$

Note that the deepest cut geometry $\mathcal{A}_{dc}^{(3)}$ is the union of these two regions with the *same* orientation, but the actual result of taking boundaries of boundaries of boundaries requires the regions to have opposite orientation separated by an internal boundary. Also note that we made a choice of which loop lines to intersect first and which to slide etc. and one might expect different choices to give different results. This is indeed the case at higher loops. At three loops however the resulting geometry (77) is the unique geometry one obtains from approaching the all-in-one-point cut.

So to summarise we find that the all-in-one-point cut as computed as a residue corresponds to two regions of opposite orientation separated by an internal boundary. At higher loops it turns out that the all-in-one-point cut is no longer even unique but depends on the precise sequence of codimension 1 boundaries taken to reach it.

4.3 Higher loop all-in-one-point cut

We commented that at three loops the multiple residue leading to the all-in-one-point cut is unique and the corresponding geometry given by (77). For higher loops, however, there are a number of inequivalent resulting geometries depending on the sequence of single residues taken. Here, we generalise the discussion of the previous section to give the inequalities associated to any all-in-one-point cut for any loop. We show that while the final configuration is always the same – that is L lines intersecting in a point – distinct paths to reach this configuration can carve out different oriented regions.

Enforcing that a line in 3d (which has four degrees of freedom) intersects a specified point kills two degrees of freedom. Thus making all L lines go through a specified point would reduce by $2L$ degrees of freedom. However the intersection point itself A is not fixed and has 3 degrees of freedom, thus only $2L - 3$ degrees of freedom are lost, corresponding to taking $2L - 3$ single residues. We distinguish between two types of residue, each of which has a different geometrical interpretation. The first is the intersection of two loop lines which are currently not connected by any set of intersecting lines (see figure 3 on the left). Taking the maximal possible number of such intersections results in a maximal tree configuration.[10] These we will refer to simply as *intersections*. The second type occurs when we merge two separate intersection points along a line (see figure 3 on the right) which we shall call a *sliding*. An all-in-one-point cut then consists of $(L-1)$ intersections and $(L-2)$ slidings to make a total of $2L - 3$.

To perform an intersection, for example $(A_iB_i) \cap (A_jB_j)$ depicted on the left in figure 3, we parameterise the point A_j as $A_j = A_i + aB_i + bZ_*$ and take the residue $b = 0$. Similarly to the discussion at three loops leading to (66), any such intersection saturates one positivity condition, $\langle A_iB_iA_jB_j \rangle = 0$, and does not generate any new inequalities. The order in which these are performed is also not important. The all-in-one-point cut consists of $L - 1$ intersections, therefore $(L-1)$ of the $(2L-3)$ mutual positivity conditions are trivialised and no new inequalities arise.

---

[10]More precisely the graph obtained by replacing each loop line with a vertex joined by edges if and only if the respective loop lines intersect should be a maximal tree on L vertices.
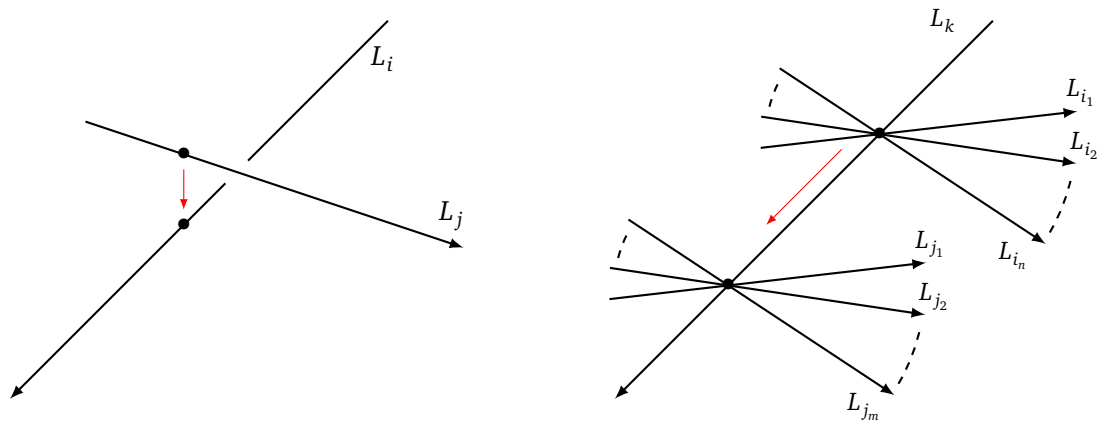
Figure 3: A graphical representation of the two types of residues discussed here. On the left is an intersection between lines L_i and L_j, which we label as (i, j). On the right is a sliding between the sets of lines $L_{i_1}, L_{i_2}, ..., L_{i_n}$ and $L_{j_1}, L_{j_2}, ..., L_{j_m}$, which we label as $(I, J) \equiv (i_1 i_2 ... i_n k, \ j_1 j_2 ... j_m k)$.

The remaining $(L - 2)$ mutual positivity conditions are handled by slidings. However, unlike the residues corresponding to the intersections, here new inequalities *are* generated. Let us begin by determining what happens when a residue is taken corresponding to a single sliding, for example the one depicted on the right in figure 3. We start off with two sets of lines intersecting at two different points, with one common loop that the two intersection points lie on.

Let I and J be the sets of labels of the two groups of intersecting lines, $k = I \cap J$ labels the line in common, and A, A' label the intersection points of the groups of lines I and J respectively, so

$$
\begin{aligned}
A &= \bigcap_{i \in I} L_i = A_k + c_1 B_k \,, \\
A' &= \bigcap_{j \in J} L_j = A_k + c_2 B_k \,.
\end{aligned}
\tag{78}
$$

In this parametrization the mutual positivity relation between loops in I and J reads

$$
\langle A_i B_i A_j B_j \rangle = (c_2 - c_1)\langle A_k B_i B_k B_j \rangle > 0, \qquad \text{for all} \ \ i \in I, \ j \in J \,.
\tag{79}
$$

As in the three loop case, the brackets factorize, giving rise to two almost disconnected regions (see (77). The geometric sliding residue is then calculated by taking the limits $(c_2 - c_1) \to 0^{\pm}$, leaving two regions with opposite orientation. A "positive" region for which $\langle A_k B_i B_k B_j \rangle > 0$ for all $i \in I, \ j \in J$ and a "negative" region for which $\langle A_k B_i B_k B_j \rangle < 0$ for all $i \in I, \ j \in J$.

To compute an all-in-one-point cut we must take $L - 2$ sliding residues, each of which splits the geometry of the boundary in two parts. If we label slidings by the index $a = 1, ..., L-2$ then we can identify a sub region with fixed orientation through the string $\vec{s} = \{s_1, \cdots, s_{L-2}\}$, where $s_a = \pm 1$ and keeps track of the signs of positively and negatively oriented regions. The resulting geometry is the union of these regions

$$
\begin{aligned}
\mathcal{R}^{\text{dc}} &= \bigcup_{\vec{s}} \mathcal{R}^{\text{dc}}_{\vec{s}} \,, \\
\mathcal{R}^{\text{dc}}_{\vec{s}} &= \mathcal{A}^{(L)}_{dc} \cap \left\{ A, B_i : s_a \langle A B_i B_{k_a} B_j \rangle > 0, \quad a = 1, .., L-2, \ i \in I_a, \ j \in J_a \right\} , \\
&\qquad \text{orientation of} \ \mathcal{R}^{\text{dc}}_{\vec{s}} = \prod_a s_a \,,
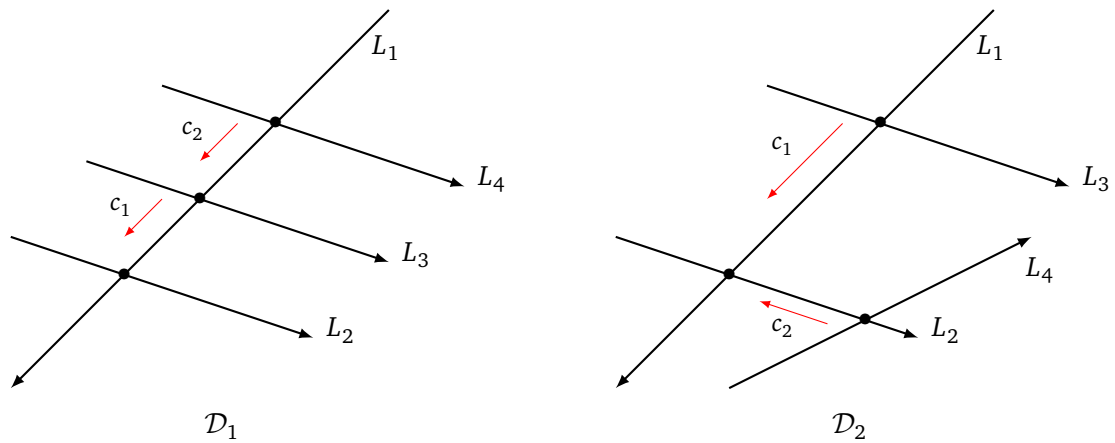\end{aligned}
\tag{80}
$$

Figure 4: Graphical representation of the four loop all-in-one-point cut labelled in (81). The all-in-one-point cut corresponds to drawing a tree configuration, and collapsing the graph so that only one intersection point remains. The *intersections* are given by pairs of intersecting lines L_i, L_j. The *slidings* are labelled in the order they should be done, $c_1, ..., c_{L-2}$. Each slide corresponds to moving one intersection point along a line in the direction dictated by the red arrow until it meets another intersection point.

where we recall that $\mathcal{A}_{dc}^{(L)}$ is the deepest cut geometry, obtained by trivialising the loop-loop inequalities of the amplituhedron and sending $A_i \rightarrow A$ (72). In particular this region depends explicitly on the sequence of boundaries we took to approach the geometry through the sets I_a, J_a.

Note that (80) generalises directly to describe the all-in-one-point cut geometry for amplituhedrons at any number of points. One just needs to add a $Y \in Gr(k, k+4)$ into each bracket and modify $\mathcal{A}_{dc}^{(L)}$ appropriately.

Example: Four loop all-in-one-point cuts

Let us illustrate (80) by giving an explicit example at four loops. Each 4 loop all-in-one-point cut is given by 3 intersections and 2 sidings. Denoting the intersection between lines L_i and L_j by (i, j) and a sliding between the sets of lines I and J as (I, J), we explore the cut

$$\{(1, 2), (1, 3), (1, 4) \, ; \, (12, 13), (123, 14)\} \, , \tag{81}$$

represented in Figure 4a. From (80), the resulting geometry is given by a union of four regions:

$$
\begin{aligned}
\mathcal{R}_1(\mathcal{D}_1) &= \mathcal{A}_{dc}^{(L)} \wedge \langle AB_2 B_1 B_3 \rangle > 0 \wedge \langle AB_2 B_1 B_4 \rangle > 0 \wedge \langle AB_3 B_1 B_4 \rangle > 0 \, , \ + \, , \\
\mathcal{R}_2(\mathcal{D}_1) &= \mathcal{A}_{dc}^{(L)} \wedge \langle AB_2 B_1 B_3 \rangle < 0 \wedge \langle AB_2 B_1 B_4 \rangle > 0 \wedge \langle AB_3 B_1 B_4 \rangle > 0 \, , \ - \, , \\
\mathcal{R}_3(\mathcal{D}_1) &= \mathcal{A}_{dc}^{(L)} \wedge \langle AB_2 B_1 B_3 \rangle > 0 \wedge \langle AB_2 B_1 B_4 \rangle < 0 \wedge \langle AB_3 B_1 B_4 \rangle < 0 \, , \ - \, , \\
\mathcal{R}_4(\mathcal{D}_1) &= \mathcal{A}_{dc}^{(L)} \wedge \langle AB_2 B_1 B_3 \rangle < 0 \wedge \langle AB_2 B_1 B_4 \rangle < 0 \wedge \langle AB_3 B_1 B_4 \rangle < 0 \, , \ + \, ,
\end{aligned}
\tag{82}
$$

where A denotes the final point that all loops intersect, and the orientation of the regions is indicated on the right by a '+' or '−'. In particular, $\mathcal{R}_1$, $\mathcal{R}_4$ have the same orientation and $\mathcal{R}_2$, $\mathcal{R}_3$ have the same orientation but opposite to $\mathcal{R}_1$, $\mathcal{R}_4$.

We see that this four loop all-in-one-point cut geometry has an internal boundary at $\langle AB_2 B_1 B_3 \rangle = 0$ and external boundaries at $\langle AB_2 B_1 B_4 \rangle = 0$, $\langle AB_3 B_1 B_4 \rangle = 0$. The corresponding multiple residue has poles in these positions.

Recall that at 3 loops all possible ways of reaching the all-in-one-point cut configuration result in the same geometry (77). At 4 loops on the other hand there are twelve different possible geometries. They are all equivalent to each other up to permutations. That is they are all given by (82) after permuting the B_i (permuting B_2, B_3 in (82) gives back the same geometry up to swapping the overall orientation and so there are only 12 inequivalent permutations rather than 24).[11] Thus the corresponding action of taking residues on a permutation invariant object such as the loop integrand yields the same result for all twelve four-loop all-in-one-point cuts. From 5 loops however there are genuinely different all-in-one-point cuts giving different results when the corresponding residues are taken on a permutation invariant object.

5 All-in-one-point-and-plane cuts

One of the attractive features of the deepest cut defined in [18] was that its canonical form was defined by a simple formula at all loops. This was because the all-in-one-point configuration (72) consists of L independent one loop inequalities and no loop-loop inequalities and the resulting geometry thus factorises. We have seen however that any action of taking consecutive boundary components to reach the deepest cut configuration gives non-unique geometries which are more involved than (72) and in particular new loop-loop inequalities of the form $\langle AB_i B_j B_k \rangle > 0$ are generated, spoiling this factorisation. The presence of these brackets makes the computation of the canonical form much more challenging and also dependent on the particular sequence off boundaries taken to reach all-in-one-point configuration.

In this section we will show that despite this complication it can still be possible to find fairly simple all loop geometries by taking further residues after reaching the all-in-one-point cut configuration that trivialize all the new $\langle AB_i B_j B_k \rangle$ inequalities. The further cuts constrain the loop lines to all lie in the same plane as well as going through the same point. They are thus simultaneously all-in-one-point and all-in-one-plane cut configurations. We will thus refer to them as all-in-one-point-and-plane cuts or point-and-plane cuts for short. They are defined in terms of the point A which all loop lines go through together with the plane $(AP_1 P_2)$ which all loop lines lie on. It is useful also to project through the point A and thus reduce the geometry to 2d, in which case we refer to the plane P instead as a line.

If we project through the common intersection point A, the geometry of the cut correspond to L points B_i on an oriented line P in $\mathbb{P}^2$. Starting at 4 loops, the $\langle AB_i B_j B_k \rangle$ inequalities force some ordering between the points on P. As a practical consequence, this implies that an all-in-one-point-and-plane cut can itself also have further loop-loop type boundaries at $B_i = B_j$. Thus taking the residues / boundaries on these effectively reduces the number of free loop variables further. We call a cut for which we have exhausted all loop-loop type residues a *maximal loop-loop* cut. All the maximal loop-loop cuts that we have considered correspond – up to a permutation of the Bs and an integer factor arising from the number of internal boundaries taken in reaching there – to the three loop maximal loop-loop cut (which is also the unique all-in-one-point-and-plane cut)

$$\mathcal{A}_{\text{mll}}^{L=3} = \left\{ A, P, B_i = P_1 + b_i P_2 : \langle AB_i \bar{j}\bar{k} \rangle > 0 : \quad i = 1, 2, 3, \ 1 \le j < k \le 4 \right\}. \tag{83}$$

We conjecture this to hold in general, that is the maximal loop loop cut always reduces to the three loop one, $\mathcal{A}_{\text{mll}}^{L} = \mathcal{A}_{\text{mll}}^{L=3}$.

In this section we will show how to compute the geometry and the canonical form of the all-in-one-point-and-plane cut from the amplituhedron. We will start with the 2 and 3 loop cases, which contain all the main features of the problem. Then we will look at the geometry

---

[11]The choice of all-in-one-point cut $\mathcal{D}_2 = \{(1, 2), (1, 3), (2, 4) ; (12, 13), (123, 24)\}$ illustrated in figure 4b looks like a different case at first sight but in fact results in the same geometry as (82) after permuting B_1 and B_2.

of the only 2 independent (up to permutations of the loop lines) all-in-one-point-and-plane cuts at 4 loops, and finally we will define a particular cut at arbitrary loops and compute its canonical form.

5.1 All-in-one-point-and-plane canonical form at 2 loops

At higher loops one can take further boundaries of the all-in-one-point configuration so that the lines all lie in a single plane. But at two loops we only have two lines intersecting in a point so they automatically lie in the same plane. Thus the all-in-one-point and the all-in-one-point-and-plane cases are identical. Nevertheless it is useful to rewrite the two loop all-in-one-point case in the same variables we will use at higher loops, namely in terms of a single line P in $\mathbb{P}^2$ (after projection through A) on which the B_is lie (each now with 1 degree of freedom).

At two loops the all-in-one-point cut is obtained simply by taking the residue in $\langle A_1 B_1 A_2 B_2 \rangle$ of (91) and is thus given by

$$
\mathcal{A}_{dc}^{(2)} = \frac{\langle AB_1 d^2 B_1 \rangle \langle AB_2 d^2 B_2 \rangle \langle 1234 \rangle^3 \langle Ad^3 A \rangle}{\langle AB_1 14 \rangle \langle AB_1 12 \rangle \langle AB_2 23 \rangle \langle AB_2 34 \rangle} \left[\frac{1}{\langle AB_1 34 \rangle \langle AB_2 12 \rangle} + \frac{1}{\langle AB_1 23 \rangle \langle AB_2 14 \rangle} \right] + B_1 \leftrightarrow B_2 .
$$

(84)

The deepest cut formula of [18] is however a completely different-looking yet identical formula for $\mathcal{A}_{dc}^{(2)}$ obtained by computing the canonical form of its corresponding geometry (72) (we recall that at two loops this correctly reproduces the corresponding residue but not beyond).
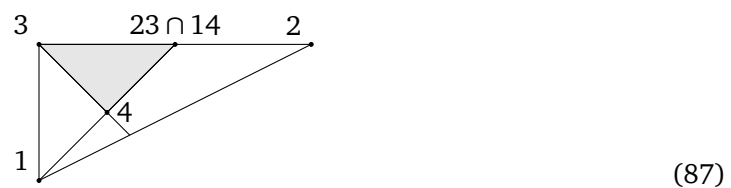
Following [18], the first step in computing the canonical form is to triangulate the A geometry into regions where the brackets $\langle Aijk \rangle$ have a well defined sign. Let's derive such a tiling for the intersection point $A = A_1 B_1 \cap A_2 B_2$. Since the intersection point A can occur at any point along a loop line, the allowed space for A can be computed as the linear combination $A = c_1 A_1 + c_2 B_1$, where $A_1 B_1$ lives in the amplituhedron. Notice, that the intersection point A is defined up to a sign, so we can fix for example $c_1 > 0$. Solving the inequalities one finds that the allowed regions for A correspond to 4 twisted cyclic permutations[12] of the solution

$$
\langle A123 \rangle > 0, \quad \langle A124 \rangle > 0, \quad \langle A134 \rangle < 0, \quad \langle A234 \rangle > 0 .
$$

(85)

All these cyclically related A regions are tetrahedra, and their canonical forms $\omega_i(A)$ (where we assign the label $i = 1$ to region (85) and the other values to its cyclic twisted permutations) can be written as $\omega_i(A) = (-1)^i \omega(A)$, with

$$
\omega(A) = \frac{\langle Ad^3 A \rangle \langle 1234 \rangle^3}{\langle A123 \rangle \langle A234 \rangle \langle A134 \rangle \langle A124 \rangle} .
$$

(86)

We can now project through A onto a plane not containing A and the remaining geometry is two dimensional. The configuration of Z_i arising from (85) is such that $1, 2, 3$ form an anti-clockwise oriented triangle containing 4:

(87)

Now we can analyze the B inequalities

$$
\langle AB14 \rangle > 0, \quad \langle AB23 \rangle > 0, \quad \langle AB34 \rangle > 0, \quad \langle AB12 \rangle > 0,
$$

(88)

---

[12] $Z_i \to Z_{i+1}$ for $i = 1, 2, 3$ and $Z_4 \to -Z_1$.

which one can see puts B inside the shaded triangle in (87), with vertices $\{4,3,(23)\cap(14)\}$. For general i after cycling we have that the B_i are in the triangle with edges $(i+2\,i+3),(i\,i+4),(i+1\,i+2)$ and vertices

$$W_{i1} = i+2, W_{i2} = i+3, W_{i3} = (i+1\,i+2)\cap(i\,i+3). \tag{89}$$

For fixed i, our problem now simply reduces to computing the canonical form of two points B_1 and B_2 living independently inside the triangle $(W_{i1}W_{i2}W_{i3})$. Each point B_i thus has the canonical form of a triangle and we obtain the two loop deepest cut form as

$$\mathcal{A}_{dc}^{(2)} = \sum_{i=1}^{4} \frac{(-1)^i \langle Ad^3A\rangle\langle 1234\rangle^3}{\langle A123\rangle\langle A234\rangle\langle A134\rangle\langle A124\rangle} \prod_{L=1}^{2} \frac{\langle AB_L d^2B_L\rangle\langle AW_{i1}W_{i2}W_{i3}\rangle^2}{\langle AB_L W_{i1}W_{i2}\rangle\langle AB_L W_{i2}W_{i3}\rangle\langle AB_L W_{i3}W_{i1}\rangle}. \tag{90}$$
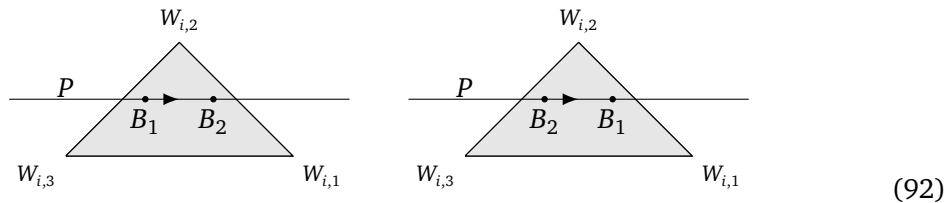
Remarkably, this is indeed equal to (84).

But we now wish to rewrite this further in a way appropriate for the higher loop all-in-one-point-and-plane cut. So instead of considering the B_i living in 2d, we consider first fixing a line P and then two points B_1', B_2' living on the 1d line P.

The Jacobian of the transformation from B_1, B_2 to P, B_1', B_2' is given by

$$\langle AB_1 d^2B_1\rangle\langle AB_2 d^2B_2\rangle = \frac{\langle AZ_*B_1'B_2'\rangle\langle AZ_*B_1'dB_1'\rangle\langle AZ_*B_2'dB_2'\rangle\langle APdP_1\rangle\langle APdP_2\rangle}{\langle AZ_*P\rangle^3}, \tag{91}$$

where Z_* is a fixed element of $\mathbb{P}^3$ such that $\langle AB_1B_2Z_*\rangle \neq 0$. Notice that the 2-loop deepest cut is symmetric in B_1 and B_2, but becomes anti-symmetric in B_1', B_2'. This corresponds geometrically to the fact that switching B_1, B_2 flips the orientation of the configuration on the right. We will shortly see how this symmetry is reflected in the amplituhedron geometry in the new variables. From now on we will drop the primes on the B_is.

The task is now to translate the geometry of two points in a triangle to that of a line through a triangle and two points on that line. We start by observing that the geometry of a line through a triangle can be triangulated into 3 regions. These correspond to the combination of the 3 ways in which the line P can intersect the edges of the triangle. However it will turn out that we also need to consider which side B_1 is of B_2 (due to the orientation switch mentioned above) and so we in fact need to split into 6 regions.

$$\tag{92}$$

Let's consider one of these 6 regions, the one on the left in (92). It is described by the inequalities

$$\langle PW_{i,1}\rangle > 0, \quad \langle PW_{i,2}\rangle < 0, \quad \langle PW_{i,3}\rangle > 0,$$
$$\langle B_l W_{i,j}W_{i,j+1}\rangle > 0, \quad \text{with} \quad j=1,2,3, \text{ and } l=1,2, \quad \langle W_{i,2}B_1B_2\rangle < 0, \tag{93}$$

with the last inequality ensuring that B_1 and B_2 are ordered.

Then all 6 configurations can be generated by cyclic permutations of (93) together with $B_1 \leftrightarrow B_2$. We will use $p = 1,2,3$ to label the cyclic permutations of (93), with $p=2$ corresponding to the case (93).

The canonical form $\lambda_{i,p}(P)$ corresponding to a line through the triangle is the same for all $p = 1, 2, 3$ and equal to

$$\lambda_{i,p}(P) = \lambda_i(P) = -\frac{\langle P \mathrm{d}P_1 \rangle \langle P \mathrm{d}P_2 \rangle \langle W_{i,1} W_{i,2} W_{i,3} \rangle}{\langle P W_{i,1} \rangle \langle P W_{i,2} \rangle \langle P W_{i,3} \rangle}, \qquad \text{with } p = 1, 2, 3. \tag{94}$$

For fixed i and p, the geometry of B_1 and B_2 corresponds to two points living on the segment with vertices $I_{i,p} = (W_{i,p-1} W_{i,p}) \cap P$ and $J_{i,p} = (W_{i,p} W_{i,p+1}) \cap P$.

The canonical form of a point B on a segment (IJ) in $\mathbb{P}^1$ can be written in general as

$$[I; B; J] := \frac{\langle J \mathrm{d}B \rangle}{\langle JB \rangle} - \frac{\langle I \mathrm{d}B \rangle}{\langle IB \rangle} = \frac{\langle B \mathrm{d}B \rangle \langle IJ \rangle}{\langle BI \rangle \langle JB \rangle}. \tag{95}$$

For our application the 1d segment lives in $\mathbb{P}^2$ (well really in $\mathbb{P}^3$ but we already projected through A onto P^2). We can choose any point to project onto the segment, call this Z_*,[13] then all the two brackets in the above formula can be viewed as 3-brackets with an additional Z_* and in turn eventually as 4-brackets with an additional A (so eg $\langle B \mathrm{d}B \rangle = \langle Z_* B \mathrm{d}B \rangle = \langle A Z_* B \mathrm{d}B \rangle$ etc.)

Then, the canonical form for B_1, B_2 ordered on the segment (IJ), with $I < B_1 < B_2 < J$ can be written as

$$[I; B_1, B_2; J] := [I; B_1; J][B_1; B_2; J] = [I; B_1; B_2][I; B_2; J], \tag{96}$$

and similarly for arbitrary numbers of ordered B_i on (IJ) we define inductively

$$[I; B_1, .., B_L; J] := [I; B_1, .., B_{L-1}; J][B_{L-1}; B_L; J]. \tag{97}$$

Now we claim that the canonical form for two free points B_1, B_2 in a triangle translates as follows

$$\prod_{l=1}^{2} \frac{\langle A B_l \mathrm{d}^2 B_l \rangle \langle A W_{i1} W_{i2} W_{i3} \rangle^2}{\langle A B_l W_{i1} W_{i2} \rangle \langle A B_l W_{i2} W_{i3} \rangle \langle A B_l W_{i3} W_{i1} \rangle} = \lambda_i(P) \sum_{p=1}^{3} \Big([I_{ip}; B_1, B_2; J_{ip}] - [I_{ip}; B_2, B_1; J_{ip}] \Big). \tag{98}$$

Note in particular the minus sign between the canonical forms for the two orderings of B_1, B_2. This is because the orientation flips when B_1 passes through B_2 as discussed below (91).

We can finally put all the pieces together and write the canonical form $\mathcal{A}_{dc}^{(L)}$ in terms of these variables as

$$\mathcal{A}_{dc}^{(2)} = \omega(A) \sum_{i=1}^{4} (-1)^i \lambda_i(P) \sum_{p=1}^{3} \Big([I_{ip}; B_1, B_2; J_{ip}] - [I_{ip}; B_2, B_1; J_{ip}] \Big). \tag{99}$$

An interesting aspect of this formula is that each term in the sum has a pole at $B_1 = B_2$. For i, p fixed this represent an internal boundary of the geometry. The sum of the residues over p though, as expected from (84), is equal to zero, which means that this pole is actually a spurious one. Geometrically, we have that when the only two points on P coincide the latter can rotate unconstrained on the pivotal point $B_1 = B_2$ and therefore its canonical form will be zero.

---

[13]Note that a natural point to choose for Z_* is the intersection point of the two edges that P is passing through, $W_{i,p}$. Then the intersection points $I_{ip} \sim W_{i,p-1}$ and $J_{ip} \sim W_{i,p+1}$ and thus the formulae dramatically simplify.

5.2 3-loops all-in-one-point-and-plane canonical form

We can now generalize the two loop result to higher loops. To compute the canonical form of a point-plane cut, we triangulate the A and P geometry in the same way we did for the two loop case and then we consider the position of Bs on the line P. The general structure of the canonical form of a specific point-plane cut will depend on the details of how the cut is taken, but it will always have the general form

$$\mathcal{A}^{(L)}_{\text{point-plane}} = 2^{n_I} \omega(A) \sum_{i=1}^{4} (-1)^i \lambda_i(P) \sum_{p=1}^{3} \sum_{\sigma \in S_L} c_\sigma \times [I_{ip}; B_{\sigma_1}, .., B_{\sigma_L}; J_{ip}], \qquad (100)$$

where $c_\sigma = \pm 1, 0$ reflecting the orientation (or absence) of a certain ordering of the $B_i s$ and where n_I is the number of internal boundaries approached to reach the configuration. So for example the two loop case (99) takes this form with $c_{\text{id}} = 1$ and $c_{(12)} = -1$. Turning to the three loop case then, we find, by direct computation of the residues, that the point-plane cut is given by (100) with $c_\sigma = 1$ for all 6 permutations $\sigma \in S_3$. Thus unlike the two loop case, for this case, the order of the $B_l s$ on the line P is not relevant and the canonical form simplifies to that of the product of three $B_l s$

$$\mathcal{A}^{(3)}_{\text{point-plane}} = 2\omega(A) \sum_{i=1}^{4} (-1)^i \lambda_i(P) \sum_{p=1}^{3} \prod_{l=1}^{3} [I_{i,p}; B_l; J_{i,p}]. \qquad (101)$$

Let us then see how this arises from the geometry. As we saw in section 4.2, the three loop all-in-one-point cut geometry is given by (77). In particular, we have a positively oriented region for $\langle AB_1B_2B_3 \rangle > 0$ and a negatively oriented region for $\langle AB_1B_2B_3 \rangle < 0$. Now consider fixing the line P (with B_1 and B_2 lying on P) and fixing B_3. Now consider passing B_1 through B_2 on the line P. As we saw in the two loop case the orientation for the geometry involving B_1, B_2 will swap, but simultaneously $\langle B_1B_2B_3 \rangle \to -\langle B_1B_2B_3 \rangle$ and so the overall orientation will also swap (see (77)). The result is no orientation change at all. We are now interested in the geometry of the internal boundary $\langle AB_1B_2B_3 \rangle = 0$ so moving B_3 also onto the line P. The point B_3 is free to go anywhere on the line P (inside the triangle). The resulting geometry is indeed just that of three free points on the line P with the canonical form (101), including the factor of 2 from taking an internal boundary.

Notice that in this case there are no remaining singularities of the form $B_i \to B_j$ so $\mathcal{A}^{(3)}_{\text{point-plane}}$ also represents what we call a maximal loop-loop cut and $2\mathcal{A}^{L=3}_{\text{mll}} := \mathcal{A}^{(3)}_{\text{point-plane}}$.

5.3 All 4-loop point-plane and maximal loop-loop cuts

We have seen that at 3-loops the all-in-one-point-and-plane cut is unique (101). At 4-loops this is not true anymore and we can have two types of geometry (modulo permutations) resulting from approaching the point-plane configuration in different ways. Each will be characterized algebraically by different coefficients c_σ in (100) and geometrically by different ordering constraints of the Bs on the line P.

We start with the all-in-one-point cut which is unique up to permutations of the loop lines and the resulting geometry given by (82). We now consider taking further boundaries of this geometry so the loops also lie in a plane. There are 3 possible loop-loop boundaries, $\langle AB_2B_1B_3 \rangle = 0$, $\langle AB_2B_1B_4 \rangle = 0$ and $\langle AB_3B_1B_4 \rangle = 0$. We start by looking at the geometry of the boundary when B_3 lies on the line P (on which B_1, B_2 lie) followed by the boundary of that geometry found when B_4 also approaches P (shortly we will switch the order of in which we take these boundaries).

The resulting geometry is of the four points B_i on the line P inside the triangle, with the following restrictions: B_1 is not allowed to be between B_2 and B_3 and the orientation depends on the relative position of B_1 and the pair B_2, B_3 (with the position of B_4 unconstrained). This geometry is derived in appendix D.

The cut resulting from this geometry is then given by the general form (100) with

$$
n_I = 2, \qquad c_\sigma = \begin{cases} 1, & \sigma = (2,3,1) \shuffle (4) \text{ or } (3,2,1) \shuffle (4), \\ -1, & \sigma = (1,2,3) \shuffle (4) \text{ or } (1,3,2) \shuffle (4), \\ 0, & \sigma = (2,1,3) \shuffle (4) \text{ or } (3,1,2) \shuffle (4), \end{cases} \tag{102}
$$

where $\shuffle$ is the shuffle operation (thus 4 can appear in any position). We have checked this is indeed correct by explicitly taking the corresponding residues of the 4 loop amplitude and finding perfect agreement.

Now note that even after taking the all-in-one-point *and* the all-in-one-plane configuration there are still uncancelled loop-loop poles at $B_1 = B_2$ and $B_1 = B_3$, corresponding geometrically to external boundaries.

Using the very simple residue structure of the ordered points on an interval canonical form, namely

$$
\text{Res}_{B_k \to B_j}[I; .., B_i, B_j, B_k, B_l..; J] = -\text{Res}_{B_k \to B_j}[I; .., B_i, B_k, B_j, B_l..; J] = [I; .., B_i, B_j, B_l..; J], \tag{103}
$$

one can quickly check that the residue of the four-loop point-plane cut (102) when $B_1 = B_2$ or $B_1 = B_3$ precisely reproduces the three-loop point-plane cut (101) with appropriate variables and with weight 4 instead of 2 (since this time we approached two internal boundaries, $\langle AB_2B_1B_3 \rangle = 0$ and $\langle AB_2B_3B_4 \rangle = 0$). This implies that the residue corresponding to this 4-loop maximal loop-loop boundary is equal to 2 times the all-in-one-point-and-plane 3-loop residue (C.12).

Returning to the all-in-one-point cut, we now consider the only other independent way of reaching the point-plane geometry (modulo permutation of the loop variables) by taking $\langle AB_2B_1B_4 \rangle = 0$ by sending B_4 to the line P followed by sending B_3 to the line P (the other way around to what we did above). In appendix D we again examine this carefully geometrically. The end result this time is the geometry of four points B_i unconstrained on the line P but with the overall orientation dependent on the ordering of B_1, B_2. The resulting canonical form is thus given by (100) with

$$
n_I = 1, \qquad c_\sigma = \begin{cases} 1, & \sigma = (2,1) \shuffle (3,4), \\ -1, & \sigma = (1,2) \shuffle (3,4), \end{cases} \tag{104}
$$

as we have confirmed by taking the residues explicitly and comparing.

Note that this time there is a remaining loop-loop residue apparent at $B_1 \to B_2$ (corresponding to an internal boundary). Taking the residue as above this again leads to the three loop point-plane result (101) after which no more loop loop residues are present. This final configuration corresponds to the 3-loop maximal cut $\mathcal{A}_{\text{mll}}$ with weight 2.

5.4 A cut at arbitrary loop order

We have already seen from the four loop examples of the previous section that the point-plane cut depends on how you approach the configuration. However one can give specific ways of approaching the point-plane geometry at any loop order and find the resulting cut. So we conclude this section by giving precisely such an example of a cut that can be computed at

arbitrary loop order. This means that we are now specifying an ordered set of residues and giving a closed formula for the result. The particular case is a generalisation of the second 4-loop case considered in the previous subsection.

We start defining what we call the simplest all-in-one-point cut. In this all loop lines first intersect the line $A_1 B_1$ and then they all slide to the same intersection point in the same order as their labeling. The geometry of this boundary at L loops can be obtained from (E.4) and is given explicitly in appendix E.

After taking the above all-in-one-point cut we then constrain all loops to lie on the same line P, first B_1, B_2 then $B_L, B_{L-1}, .., B_3$ thus taking the ordered series of boundaries $\{\langle AB_2 B_1 B_L \rangle = 0, \langle AB_2 B_1 B_{L-1} \rangle = 0, \cdots, \langle AB_2 B_1 B_3 \rangle = 0\}$.

Carefully examining the resulting geometry as is done explicitly in appendix E, we arrive at the final geometry corresponding to this point-plane cut. It is given by L points B_i lying on the line P, with B_3, B_L unconstrained and with B_1 always lying between B_2 and all of the points $B_4, .., B_{L-1}$. The orientation of the geometry depends on the relative order of B_1, B_2. The resulting canonical form at arbitrary loop order is thus

$$\mathcal{A}_{\text{point-plane}}^{(L)} = 2 \sum_{i=1}^{4} \omega(A) \sum_{p=1}^{3} \lambda_{i,p}(P)[I_{i,p}; B_3; J_{i,p}][I_{i,p}; B_L; J_{i,p}]$$
$$\times \left([I_{i,p}; B_2, B_1; J_{i,p}] \prod_{l=4}^{L-1}[B_1; B_l; J_{i,p}] + (-1)^{L-1}[I_{i,p}; B_1, B_2; J_{i,p}] \prod_{l=4}^{L-1}[I_{i,p}; B_l; B_1] \right).$$
(105)

We tested (105) by computing this simplest maximal loop-loop residue up to 7 loops from the explicit from of the amplitude obtained in [22] and found complete agreement. We see that this point-plane cut has further poles when $B_l \to B_1$. We have checked up to 5 loops that taking further residues in these poles eventually leads to the 3 loop point-plane cut (101). Indeed our investigations so far indicate that after taking any all-in-one-point-and-plane geometry at any loop order, there are always $L-3$ boundaries of the form $B_i \to B_j$ remaining. After further taking these boundaries we are then always lead to the three loop point-plane geometry (101). It might be possible to prove this starting from the explicit all-in-one-point geometry (80).

6 Conclusions

We summarise the main points of the paper and point out topics for further work.

We began by observing that non-vanishing maximal residues of loop amplitudes are not always ± 1 as has generally been assumed, but can take arbitrary values in $\mathbb{Z}$, apparently contradicting the fact that the loop amplituhedron is a positive geometry. We found the source of this apparent contradiction geometrically to be the existence of *internal boundaries* in the geometry where two regions of opposite orientation touch. This minimally requires including an extra term in the recursive definition of the canonical form to take into account these internal boundaries (22). In all the examples we have found, the internal boundaries arise from loop-loop propagators factorizing into the product of two factors. Algebraically these are examples of composite residues discussed in this context in [9] and it would be interesting to explore the relation between composite residues and internal boundaries in more detail.

As well as internal boundaries we have also stressed another under emphasised feature of the boundary structure of the amplituhedron and multiple residues, namely the simple fact that multiple-residues and corresponding multiple boundaries are non-unique. On the algebraic side a multiple residue is defined as an (ordered) sequence of simple residues. In the same way, on the geometrical side the relevant quantity one must use is 'boundaries of

boundaries of...' rather than 'codimension k boundaries'. It would be interesting to revisit previous computations of the boundary structure of the loop amplituhedron, and in particular its genus, for example [16], taking into account both internal boundaries and the above non uniqueness of codimension k boundaries.

These two features of the amplituhedron, internal boundaries and ambiguity of multiple boundaries, come into sharp focus when investigating the deepest cuts of [18]. The all loop formulae for these cuts described there is not obtainable directly by taking multiple single residues of the amplituhedron due to the presence of internal boundaries. We have shown that nevertheless all-loop formulae can be obtained. They will inevitably depend though on the details of the cut taken (that is the precise sequence of simple residues taken) and they will in general contain further loop-loop poles after reaching the all-in-one-point cut configuration. We give an example of an all loop formula for a particular all in plane and point cut. It would be fascinating to obtain a general formula taking as input the details of the cut taken and as output the corresponding canonical form. In general it seems that, taking loop-loop type residues there are always available more loop-loop type poles (or boundaries) until one eventually reaches a configuration with just three loop lines (so all other loop lines coincide with one of these three) intersecting in a point and lying in a plane. This is arguably then the true 'deepest cut' or 'maximal loop-loop cut' one can take. That is to say it is the maximal cut involving only loop-loop type poles. It has a universal form given by the three loop all in plane and point cut, but with an integer valued coefficient related to the number of internal boundaries one takes in arriving there.

The four-point planar amplitude integrand in $\mathcal{N} = 4$ SYM (and its closely related half BPS correlator) is known to ten loops using various graphical rules together with correlator insights [22]. There have also been investigations o it directly using amplituhedron insights [23–25]. A key question in this context then is whether the above all-loop cuts can be used practically to actually compute the 4-point amplitude/correlator at higher loops. Taking maximal residues (eg first the all-in-one-point cut, then further external cuts) yields a vast amount of information about the amplitude. It also has the tantalising chance of being a constructive approach: rather than using a huge basis of graphs and determining their coefficients, most of which are zero, it might be possible to use the cuts to construct only the relevant graphs and non-zero coefficients with which they appear.

Although we have focused on 4 points, the all-in-one-point cut and more general loop-loop cuts are largely independent of the number of points, and also the MHV degree, since they involve only the mutual geometry between loop lines rather than the details of the external geometry. There has been some nice recent progress in computing the amplitude for arbitrary multiplicity directly from the loop amplituhedron [14, 26–28]. Points worthy of note in the current context are that taking the maximal multiple residues involving loops at higher points yields leading singularities of amplitudes – rational coefficients – which have been extensively analysed and are given by Yangian invariant Grassmann integrals [9, 29]. Furthermore in the works [4, 5] a method for extracting a list of the physical amplitude's branch points from the amplituhedron is suggested. Here the boundaries are derived by intersecting the closure of the amplituhedron with the boundary components corresponding to vanishing brackets of the form $\langle ABij \rangle, \langle A_i B_i A_j B_j \rangle$. It would be extremely interesting to revisit both the above points using the insights and technology developed here.

Unlike positive geometries, the space of generalised positive geometries is closed under union: regions that are triangulated by GPGs will be GPGs. This then suggests they might be a better arena to seek a direct characterisation – that is a simple straightforward answer to the question 'is the following region a GPG or not' – than PGs. In particular it seems clear that all multi-linear geometries are GPGs, and their canonical form can be computed algorithmically via cylindrical decomposition. Nicely all Grassmannian-type geometries, the type seen in

physics, are multi-linear geometries and thus GPGs. But this is not the most general class and the most general classification needs more investigation.

The generalisation of positive geometry to include internal boundaries also suggests the utility of a further generalisation to *weighted positive geometries* where instead the weights contain the information about internal boundaries, and the canonical form has a much more natural definition (36). This concept also makes certain proofs very direct since one can add two WPGs together without first making sure they are disjoint (see eg the proof of triangulations of positive geometries in section 3.5).

In [2, 30] the geometry of the log of the MHV amplitude is considered and defined as a union of geometries with negative mutual positivity condition $\langle A_i B_i A_j B_j \rangle < 0$. One of these has negative mutual positivity condition for all i, j and its canonical form is equal to the amplituhedron canonical form. The latter is the only term in the log of the amplitude surviving the all-in-one-point cut and therefore the all-in-one-point cut of the amplitude and the log of the amplitude are the same. The log of amplitude should most naturally be described by a WPG.

We believe that the above insights will also have utility in the increasing number of wider applications of positive geometry concepts in physics beyond the amplituhedron. One closely related case is the momentum amplituhedron. For the tree-level momentum amplituhedron [31] a lot is known about its boundary stratification [32, 33] and its Euler characteristic has been proven to be equal to one [34], a strong indication that the geometry is free from internal boundaries. However, despite the very solid understanding achieved at tree level, finding the geometry of the loop momentum amplituhedron remains an open problem. In this case we expect internal boundaries to appear and the language of WPGs could give the right framework to define a loop momentum amplituhedron. Also in the search for a non-planar amplituhedron interesting ideas involving the sum of geometries over different orderings have been explored in [35, 36] and might benefit from being viewed as weighted positive geometries. Other wider applications of positive geometry which one could revisit include [37–44]. Similarly weighted positive geometry may provide the right mathematical framework to deal with cosmological correlators, which contrarily to the wavefunction of the universe described by the cosmological polytopes [45,46]s, do not currently have a geometrical description. Their maximal residues are not $+/-$ 1 and they naively appears as a weighted sum of canonical forms of cosmological polytopes (P. Benincasa, private communication).

Acknowledgments

A Inducing orientations on boundary manifolds

Here we would like to review how given an oriented manifold one can derive the induced orientation of the boundary. An oriented manifold $\mathcal{M}$ is oriented if it posses a continuous top differential form $\mathcal{O}$ that is always non-vanishing in $\mathcal{M}$. The orientation is then equivalently defined by this volume form modulo positive scaling. Suppose then $\mathcal{M}$ has a boundary $\partial\mathcal{M}$ of codimension one. The orientation ω_∂ induced by $\mathcal{O}$ on $\partial\mathcal{M}$ will be the projection of $\mathcal{O}$ on $\partial\mathcal{M}$. We will now define what we mean by projection. Let the boundary be defined by $f = 0$ with $f > 0$ inside and $f < 0$ outside the region (at least near by). Then $\mathcal{O}_\partial$ is defined simply as

$$df \wedge \mathcal{O}_\partial = \mathcal{O}|_{\partial\mathcal{M}}. \tag{A.1}$$

Note that the standard convention in math literature differ by a sign, that is df represents an outward pointing differential. We make this choice so that the segment $x > 0$ with positive orientation form $O(x) = dx$ has orientation $O|_{x=0} = 1$. In this way the canonical form of the positively oriented segment is $\Omega(x > 0, dx) = \frac{dx}{x}$, in fact this form satisfies

$$\mathrm{Res}_{x=0}\left(\frac{dx}{x}\right) = O|_{x=0} = 1. \tag{A.2}$$

B Relation of generalised positive geometries to the globally oriented canonical form

The globally oriented canonical form was defined in [11] to obtain the square of the super amplitude out of the geometry of the squared amplituhedron. The interior of the squared amplituhedron consists of several disconnected components so the first problem is to define the relative orientation of these components. The second problem is that the square of the super-amplitude has non-normalizable maximal residues and therefore can not be possibly interpreted as a canonical form of a positive geometry. We solved both problems by noticing that the GCD algorithm (see [11, 20]) correctly reproduces the canonical form of the squared amplituhedron. The GCD algorithm works in coordinates, that is on a $\mathbb{R}^{km}$ patch of the oriented Grassmannian using the tiling property of canonical forms. The orientation of the subregions given by the GCD are fixed by the algorithm as the global orientation of the coordinate patch. Then it gives the result as the sum of the canonical forms of the positive geometries triangulating the region. We then defined the oriented canonical form as the sum of the canonical form of the regions triangulating the squared amplituhedron.

With the new concept we introduced in this paper, we can simply say then that the squared amplituhedron is a GPG with the orientation fixed by the global orientation of the oriented Grassmannian. The canonical form of a generalized positive geometry $X_{\geq 0}$ in an orientable space X with orientation coinciding with the orientation of X is equal to its globally oriented canonical form.

C Three loop internal boundary and its maximal residues

Here we consider taking further residues of the all-in-one-point cut (68) to eventually arrive at the leading singularities. Then we will consider the same sequence geometrically. Indeed in [21] such maximal residues were considered leading to a final configuration in which all loop lines intersect external twistors as well as intersecting each other at a single point A.

Specifically we consider the case where loop line L_1 intersects Z_1 and L_2, L_3 intersect Z_2. We here show that the resulting residue depends on the path taken. Furthermore if the path taken involves taking a residue in $\langle AB_1B_2B_3\rangle = 0$ first, then the resulting maximal residue has magnitude 2 suggesting that $\langle AB_1B_2B_3\rangle = 0$ corresponds to an internal boundary.

The two routes we consider to reach the above configuration are as follows. For route 2 we first take further residues of the all-in-one-point cut (68) in the following order

$$\langle AB_112\rangle = 0, \quad \langle AB_114\rangle = 0, \quad \langle AB_212\rangle = 0, \quad \langle AB_223\rangle = 0. \tag{C.1}$$

This corresponds to intersecting line L_1 with the edge Z_1Z_4 and then with Z_1 followed by intersecting L_2 with the edge Z_1Z_2 and then to Z_2. In the process the pole $\langle AB_1B_2B_3\rangle \to \langle A12B_3\rangle$ and so the final step is to take residues in this pole $\langle A12B_3\rangle = 0$ followed by $\langle A23B_3\rangle = 0$ corresponding to L_3 intersecting Z_1Z_2 and then sliding to Z_2. We take the residues explicitly by parametrizing the B_i as follows (with Z_* an arbitrary twistor)

$$\begin{aligned}
B_1 &= c_1Z_4 + Z_1 + d_1Z_*, \\
B_2 &= c_2Z_1 + Z_2 + d_2Z_*, \\
B_3 &= c_3Z_1 + Z_2 + d_3Z_*,
\end{aligned} \tag{C.2}$$

and considering the residues at zero in $d_1, c_1, d_2, c_2, d_3, c_3$ in that order. The residues are straightforward to compute and can be done covariantly, for example:

$$\operatorname*{Res}_{d_1=0,\,c_1=0}\left(\frac{\langle AB_1\mathrm{d}^2B_1\rangle}{\langle AB_114\rangle\langle AB_112\rangle}\right) = \frac{-1}{\langle A214\rangle}. \tag{C.3}$$

Only the displayed term in (67) out of the 24 total terms survives this sequence of residues and it produces the final result

$$-\frac{\langle 1234\rangle^3\langle A\mathrm{d}^3A\rangle}{\langle A123\rangle\langle A124\rangle\langle A134\rangle\langle A234\rangle} = -\frac{\mathrm{d}a\,\mathrm{d}b\,\mathrm{d}c}{abc}, \tag{C.4}$$

where on the right hand side we parametrise the point A as

$$A = Z_1 + aZ_2 + bZ_3 + cZ_4. \tag{C.5}$$

This is the canonical form of a tetrahedron with vertices Z_i and is inline with the prediction of [21]. Indeed the mutual intersection point A is now the only remaining freedom and restricting the amplituhedron geometry to this configuration results in the tetrahedron. However as we saw in the simple example in the introduction, simply restricting the geometry to a high codimension boundary will not always give the right answer and the precise order in which one takes the residues can be important.

For route 2 therefore we change the order in which we take the residues on the all-in-one-point cut (68). We first take a residue in the pole $\langle AB_1B_2B_3\rangle$ making L_3 coplanar with $L1$ and $L2$. Then proceed taking residues as previously in (C.1) moving $B_1 \to Z_1$ and $B_2 \to Z_2$. Then finally we take a residue as $B_3 \to Z_2$. Explicitly then, this time we parametrize the B_i as follows

$$\begin{aligned}
B_3 &= c_3B_1 + B_2 + d_3Z_*, \\
B_1 &= c_1Z_4 + Z_1 + d_1Z_*, \\
B_2 &= c_2Z_1 + Z_2 + d_2Z_*,
\end{aligned} \tag{C.6}$$

and take the residues at zero in the order $d_3, d_1, c_1, d_2, c_2, c_3$. The first residue is

$$\operatorname*{Res}_{\langle AB_1B_2B_3\rangle=0}\left(\frac{\langle AB_3\mathrm{d}^2B_3\rangle}{\langle AB_1B_2B_3\rangle}\right) = -\mathrm{d}c_3, \tag{C.7}$$

and then use similar results to (C.3) before finally taking the residue in the parameter c_3. This time two terms in (67) survive, the displayed term together with the term

$$\frac{\langle A\mathrm{d}^3 A\rangle \prod_{i=1}^{3}\langle AB_i \mathrm{d}^2 B_i\rangle \langle 1234\rangle^3 \langle 23AB_1\rangle}{\langle 12AB_1\rangle \langle 12AB_3\rangle \langle 14AB_1\rangle \langle 23AB_2\rangle \langle 23AB_3\rangle \langle 34AB_1\rangle \langle 34AB_2\rangle \langle AB_1 B_2 B_3\rangle} \, . \tag{C.8}$$

Note that this term only survives because a required pole $\langle 12AB_2\rangle$ appears from the pole in $\langle 12AB_3\rangle$ after the residues in $d_3 = 0, d_1 = 0, c_1 = 0$ have been taken. Since there are two terms now surviving, the final result turns out to be twice (C.4)

$$-\frac{2\langle 1234\rangle^3 \langle A\mathrm{d}^3 A\rangle}{\langle A123\rangle \langle A124\rangle \langle A134\rangle \langle A234\rangle} = -2\frac{\mathrm{d}a\,\mathrm{d}b\,\mathrm{d}c}{abc} \, . \tag{C.9}$$

Now the final configuration of these two routes is exactly the same in both cases: $B_1 \to Z_1, B_2, B_3 \to Z_2$ and yet the results differ by a factor of 2. We thus clearly see the importance of path dependence when taking residues. We will shortly see that path dependence can give different results for the all-in-one-point cut itself (rather than just when taking further residues). Furthermore, taking three further residues as $a, b, c \to 0$ clearly gives us a maximal residue of magnitude 2 indicating that there is an internal boundary present. Let us then consider this geometrically.

We can now redo the above computation geometrically by taking boundaries of the all-in-one-point cut geometry (77) and using our formula of the canonical form of a GPG (22). To do this, we parametrise A and B_i just as in (C.5) and (C.6)

$$\begin{aligned}
B_3 &= c_3 B_1 + B_2 + d_3 Z_*, \\
B_1 &= c_1 Z_4 + Z_1 + d_1 Z_*, \\
B_2 &= c_2 Z_1 + Z_2 + d_2 Z_*, \\
A &= Z_1 + a Z_2 + b Z_3 + c Z_4.
\end{aligned} \tag{C.10}$$

Then take boundaries in the same order with which we took residues following (C.9)

$$d_3 = 0, \quad d_1 = 0, \quad c_1 = 0, \quad d_2 = 0, \quad c_2 = 0, \quad c_3 = 0. \tag{C.11}$$

The first boundary corresponds to the above internal boundary $\langle AB_1 B_2 B_3\rangle = 0$. Therefore, from the recursive definition of the canonical form in the presence of internal boundaries (22), the canonical form of the all-in-one-point cut geometry satisfies

$$\lim_{d_3 \to 0} d_3 \big(\Omega(\mathcal{R}_1^{\mathrm{dc}}) + \Omega(\mathcal{R}_2^{\mathrm{dc}})\big) = 2\mathrm{d}d_3 \wedge \Omega\big(\mathcal{R}^{\mathrm{dc}}|_{\langle AB_1 B_2 B_3\rangle = 0}\big) \, . \tag{C.12}$$

This simply means that the residue, $d_3 = 0$, on the canonical form determined by the inequalities describing the geometry of the all-in-one-point cut (74), is equal to twice the canonical form of the interior boundary, i.e. the canonical form determined by the inequalities (70) with $B_3 = B_1 + a_3 B_2$.

Continuing with the remaining boundaries, the final geometry is described by the following set of inequalities,

$$\mathcal{R}^{\mathrm{final}} : \quad a < 0, \quad b > 0, \quad c > 0. \tag{C.13}$$

The remaining residues were all on external boundaries, therefore the canonical form of the final region is $2\Omega(\mathcal{R}^{\mathrm{final}})$, where the factor of two comes from the internal boundary residue (C.12). The final inequalities describe a tetrahedron with vertices $\{Z_1, -Z_2, Z_3, Z_4\}$ and therefore the final canonical form is in precise agreement with (C.4).

We see that the internal boundary at $\langle AB_1 B_2 B_3\rangle = 0$ is key to obtaining the correct leading singularity from the geometry. Just as we saw algebraically above, it is also possible to

reach the same final loop configuration by only going to consecutive *external* boundaries. An example of this would be to follow the residues described in (C.2) geometrically. Then the final canonical form would be, up to an overall sign, the canonical form of the tetrahedron without the factor of two, as predicted in [21]. We see that the precise sequence of codimension 1 boundaries taken to approach higher codimension boundaries starting from the all-in-one-point cut configuration can give different results. At higher loops this is also true for the all-in-one-point cut itself (rather than just its maximal residues as here).

D   Four loop point-plane boundary geometry

We here examine the geometry of the loop-loop boundaries of the four loop all-in-one-point cut (82). We start by the boundary when B_3 lies on the line $P = B_1B_2$ followed by the boundary of that geometry when B_4 also approaches P. We observe that the regions $\mathcal{R}_1$ and $\mathcal{R}_2$ of (82) touch on $\langle AB_2B_1B_3 \rangle = 0$ as do $\mathcal{R}_3$ and $\mathcal{R}_4$. Since the orientations of $\mathcal{R}_1$ and $\mathcal{R}_2$ are opposite as are $\mathcal{R}_3$ and $\mathcal{R}_4$, this is an internal boundary. Thus the geometry of the (internal) amplituhedron boundary $\langle AB_2B_1B_3 \rangle = 0$, with B_3 living on B_2B_1, is given by $\mathcal{R}_{12} \cup \mathcal{R}_{34}$ where

$$
\begin{aligned}
\mathcal{R}_{12} &= \mathcal{A}_{dc}^{(4)} \wedge \langle AB_2B_1B_4 \rangle > 0 \wedge \langle AB_3B_1B_4 \rangle > 0|_{B_3 \in B_2B_1}, \quad +, \\
\mathcal{R}_{34} &= \mathcal{A}_{dc}^{(4)} \wedge \langle AB_2B_1B_4 \rangle < 0 \wedge \langle AB_3B_1B_4 \rangle < 0|_{B_3 \in B_2B_1}, \quad -.
\end{aligned}
\tag{D.1}
$$

Here $\mathcal{R}_{12}$ is positively oriented (indicated by the +), while $\mathcal{R}_{34}$ is negatively oriented. Notice that both of these regions require B_1 to be on the same side of B_2 and B_3. In other words B_1 can not lie between B_2 and B_3. Further the orientation depends which side of B_2, B_3, B_1 is on. Then after we send B_4 to the line P, we approach another internal boundary, with no further constraints on where B_4 can lie. We thus conclude that the geometry is of the four points B_i on the line P inside the triangle, with B_1 not allowed between B_2 and B_3 and the orientation depending on the relative position of B_1 and B_2, B_3.

We can check the geometry more carefully by exploring the boundaries of (D.1) explicitly. To do this we make the constraint $\langle AB_1B_2B_3 \rangle = 0$ explicit by expanding B_1 as $c_1B_2 + c_2B_3$. Then (D.1) becomes

$$
\begin{aligned}
\mathcal{R}_{12} &= \mathcal{A}_{dc}^{(4)} \wedge \left(\langle AB_2B_3B_4 \rangle > 0 \wedge c_1 < 0 \wedge c_2 > 0 \right) \vee \left(\langle AB_2B_3B_4 \rangle < 0 \wedge c_1 > 0 \wedge c_2 < 0 \right), \ +, \\
\mathcal{R}_{34} &= \mathcal{A}_{dc}^{(4)} \wedge \left(\langle AB_2B_3B_4 \rangle > 0 \wedge c_1 > 0 \wedge c_2 < 0 \right) \vee \left(\langle AB_2B_3B_4 \rangle < 0 \wedge c_1 < 0 \wedge c_2 > 0 \right), \ -,
\end{aligned}
\tag{D.2}
$$

and we see this has two external boundaries, $c_1 = 0$ and $c_2 = 0$, and one internal boundary at $\langle AB_2B_3B_4 \rangle = 0$. The two external boundaries correspond to sending $B_1 \to B_3$ and $B_1 \to B_2$ respectively. The limit internal boundary $\langle AB_2B_3B_4 \rangle \to 0^{\pm}$ instead corresponds to sending B_4 to the line P. In this case the geometry is described by the union of a positively oriented region $\mathcal{R}_{1234}^+$ and a negatively oriented region $\mathcal{R}_{1234}^-$ as

$$
\begin{aligned}
\mathcal{R}_{1234}^+ &= \mathcal{A}_{dc}^{(4)} \wedge c_1 < 0 \wedge c_2 > 0, \quad +, \\
\mathcal{R}_{1234}^- &= \mathcal{A}_{dc}^{(4)} \wedge c_1 > 0 \wedge c_2 < 0, \quad -.
\end{aligned}
\tag{D.3}
$$

We clearly see then recalling $B_1 = c_1B_2 + c_2B_3$ that B_1 cannot line in between the point B_2 and B_3 and the orientation depends on which side of $B2, B_3$ B_1 is on, with the position of B_4 unconstrained.

This also reveals that there are still further loop-loop type boundaries we could take even after doing the point-plane-cut. We could take a residue at $c_2 = 0$ or $c_3 = 0$ corresponding to

$B_1 = B_2$ or B_3. The geometry we then obtain corresponds to the 3-loops maximal loop-loop cut $\mathcal{A}^{(3)}_{\text{mll}}$ but with weight 4 instead of 2 since this time we approached two internal boundaries that is $\langle AB_2B_1B_3 \rangle = 0$ and $\langle AB_2B_3B_4 \rangle = 0$. This implies that the residue corresponding to this 4-loop boundary is equal to 2 times the (C.12) all-in-one-point-and-plane 3-loop residue.

Let's now go back to the all-in-one-point cut (82) and explore the only other boundary (modulo permutation of the loop variables), at $\langle AB_2B_1B_4 \rangle = 0$. Notice that this time it is an external boundary since the 4 regions remain distinct. To be very explicit, we can approach the boundary by parametrizing B_1 as $c_1B_2 + c_2B_4 + c_3Z^*$ and then taking the limit $c_3 \to 0^{\pm}$ on (82), which becomes

$$
\begin{aligned}
\mathcal{R}_1 &= \mathcal{A}^{(4)}_{dc} \wedge c_2\langle AB_2B_3B_4 \rangle > 0 \wedge -c_1\langle AB_2B_3B_4 \rangle > 0, \, +, \\
\mathcal{R}_2 &= \mathcal{A}^{(4)}_{dc} \wedge c_2\langle AB_2B_3B_4 \rangle < 0 \wedge -c_1\langle AB_2B_3B_4 \rangle > 0, \, -, \\
\mathcal{R}_3 &= \mathcal{A}^{(4)}_{dc} \wedge c_2\langle AB_2B_3B_4 \rangle > 0 \wedge -c_1\langle AB_2B_3B_4 \rangle < 0, \, +, \\
\mathcal{R}_4 &= \mathcal{A}^{(4)}_{dc} \wedge c_2\langle AB_2B_3B_4 \rangle < 0 \wedge -c_1\langle AB_2B_3B_4 \rangle < 0, \, -,
\end{aligned}
\tag{D.4}
$$

where the region 1 and 3 are positively oriented and 2 and 4 are negatively oriented. Here the geometry looks very similar to (D.2), but this time $c_1 = 0$ is unconstrained while c_2 is an external boundary. We can see that c_1 is free by taking the union of $\mathcal{R}_1$ and $\mathcal{R}_3$ and expanding the products into the different sign cases. The same goes for the pair $\mathcal{R}_2, \mathcal{R}_4$. Because of this we can actually rewrite the (D.4) as

$$
\begin{aligned}
\mathcal{R}_{13} &= \mathcal{A}^{(4)}_{dc} \wedge c_2\langle AB_2B_3B_4 \rangle > 0, \, +, \\
\mathcal{R}_{24} &= \mathcal{A}^{(4)}_{dc} \wedge c_2\langle AB_2B_3B_4 \rangle < 0, \, -.
\end{aligned}
\tag{D.5}
$$

This in turn then has two boundaries, $\langle AB_2B_1B_3 \rangle = 0$ and $c_2 = 0$. Setting $\langle AB_2B_1B_3 \rangle = 0$ obtained by sending B_3 to P is described by the union of a positively oriented region and a negatively oriented region as

$$
\begin{aligned}
\mathcal{R}^+_{1234} &= \mathcal{A}^{(4)}_{dc} c_2 > 0, \, +, \\
\mathcal{R}^-_{1234} &= \mathcal{A}^{(4)}_{dc} c_2 < 0, \, -.
\end{aligned}
\tag{D.6}
$$

This is the geometry of unconstrained points B_i with orientation depending on the relative order of B_1, B_2.

This point-plane configuration has a further (internal) loop-loop boundary at $c_2 = 0$ corresponding to the limit $B_1 \to B_2$. This boundary then consists of three unconstrained points on the line B_2, B_3, B_4. This final configuration thus corresponds to the 3-loop maximal cut $\mathcal{A}^{(3)}_{\text{mll}}$ with weight 2.

E   An all loop point-plane geometry

We here describe in detail the geometry corresponding to the specific all loop point-plane cut described in section 5.4.

We first take the simplest all-in-one-point cut boundary. In this all loops first intersect the line A_1B_1 and then they all slide to the same intersection point in the same order as their labeling. At L loops this is given by the inequalities (see (E.4))

$$
\mathcal{R}^{\text{simplest dc}} = \bigcup_{\vec{s}} \mathcal{R}^{\text{simplest dc}}_{\vec{s}},
$$

$$
\mathcal{R}^{\text{simplest dc}}_{\vec{s}} = \mathcal{A}_{\text{dc}} \wedge \left(\bigwedge_{a=3}^{L} \bigwedge_{2<i<a} \{ s_a\langle AB_iB_1B_a \rangle > 0 \} \right), \qquad \text{orientation} = \prod_a s_a.
\tag{E.1}
$$

After taking the above all-in-one-point cut we then constrain all loops to lie in the same plane by taking the ordered series of boundaries $\{\langle AB_2 B_1 B_L \rangle = 0, \langle AB_2 B_1 B_{L-1} \rangle = 0, \cdots, \langle AB_2 B_1 B_3 \rangle = 0\}$. To do this, we will parametrize all loops, but B_1 and B_2, as $B_a = B_1 + b_a B_2 + c_a Z^*$ and we will take the limit $c_a \to 0^\pm$. We start by approaching the boundary $\langle AB_2 B_1 B_L \rangle$. What we obtain after this first limit is that for all i

$$s_L \langle AB_i B_1 B_L \rangle > 0 \to s_L b_L \langle AB_i B_1 B_2 \rangle = -s_L s_i b_L < 0. \tag{E.2}$$

Since this inequality must hold for all i we have that all s_i, apart from s_L must be equal and we can therefore define a single sign s as

$$s := s_{L-1} = \cdots = s_3. \tag{E.3}$$

Moreover, we can see that b_L is actually unconstrained. In fact, since for $s_L > 0$ and $s_L < 0$ we have the same orientation, (E.2) reduces to $b_L > 0 \vee b_L < 0$. The boundary geometry is then given by

$$\mathcal{R}^{\text{simplest dc}}|_{\langle A, B_2 B_1 B_L \rangle = 0} = \mathcal{R}^{\text{simplest dc}}_{s=1}|_{\langle A, B_2 B_1 B_L \rangle = 0} \cup \mathcal{R}^{\text{simplest dc}}_{s=-1}|_{\langle A, B_2 B_1 B_L \rangle = 0},$$

$$\mathcal{R}^{\text{simplest dc}}_s|_{\langle A, B_2 B_1 B_L \rangle = 0} = \mathcal{A}_{\text{dc}} \wedge \left(\bigwedge_{a=3}^{L-1} \bigwedge_{2 < i < j} \{s \langle AB_i B_1 B_a \rangle > 0\} \right), \qquad \text{orientation} = s^{L-4}. \tag{E.4}$$

Now let's take the residue $\langle A21 B_{L-1} \rangle = 0$ by taking the limit $c_L \to 0^\pm$. What we obtain is that

$$s \langle AB_i B_1 B_{L-1} \rangle > 0 = s \langle AB_i B_1 B_2 \rangle b_{L-1} > 0 = b_L < 0. \tag{E.5}$$

This implies that $b_{L-1} \to 0^-$ corresponds to an external boundary of the geometry. Notice also that now the orientation of the two components of the geometry labeled by $s = 1$ and $s - 1$ will be given by s^{L-5}. The series of boundaries $\langle AB_2 B_1 B_a \rangle = 0$ have a clear recursive structure such that at each step a we get an inequality of the form $b_a < 0$ and the orientation of the two components is equal to s^{L-a-3}. The recursion ends when we get to the last residue on $\langle AB_1 B_2 B_3 \rangle = 0$, for which no brackets of the form $\langle AB_i B_1 B_3 \rangle$ are present. At that point the two components $\langle AB_1 B_2 B_3 \rangle > 0$ and $\langle AB_1 B_2 B_3 \rangle < 0$ have the same boundary and opposite orientation and therefore this represents an internal boundary. We can conclude that the geometry of the simplest all-in-one-plane-and-point cut corresponds to

$$\mathcal{R}^{\text{simplest dc}}_{s,L}|_{\bigwedge_a \langle A, B_2 B_1 B_a \rangle = 0} = \mathcal{A}_{\text{dc}} \wedge \left(\bigwedge_{a=4}^{L-1} b_a < 0 \right), \tag{E.6}$$

where the weight of geometry is equal to 2 due to the internal boundary $\langle AB_1 B_2 B_3 \rangle = 0$ contribution.

At this point it's straight forward to compute the canonical form of this region for the 4-point MHV amplitude. The inequalities $b_a < 0$ for $a = 4, \cdots, L-1$ simply tell us that on the line P all B_a must be on the same side of B_1 as B_2. So the full canonical form is as given in (105).

References

[1] N. Arkani-Hamed and J. Trnka, *The amplituhedron*, J. High Energy Phys. **10**, 030 (2014), doi:10.1007/JHEP10(2014)030.

[2] N. Arkani-Hamed and J. Trnka, *Into the amplituhedron*, J. High Energy Phys. **12**, 182 (2014), doi:10.1007/JHEP12(2014)182.

[3] E. Herrmann and J. Trnka, *The SAGEX review on scattering amplitudes, Chapter 7: Positive geometry of scattering amplitudes*, J. Phys. A: Math. Theor. **55**, 443008 (2022), doi:10.1088/1751-8121/ac8709.

[4] T. Dennen, I. Prlina, M. Spradlin, S. Stanojevic and A. Volovich, *Landau singularities from the amplituhedron*, J. High Energy Phys. **06**, 152 (2017), doi:10.1007/JHEP06(2017)152.

[5] I. Prlina, M. Spradlin, J. Stankowicz, S. Stanojevic and A. Volovich, *All-helicity symbol alphabets from unwound amplituhedra*, J. High Energy Phys. **05**, 159 (2018), doi:10.1007/JHEP05(2018)159.

[6] N. Arkani-Hamed, J. Bourjaily, F. Cachazo, A. Goncharov, A. Postnikov and J. Trnka, *Grassmannian geometry of scattering amplitudes*, Cambridge University Press, Cambridge, UK, ISBN 9781107086586 (2016), doi:10.1017/CBO9781316091548.

[7] R. Britto, F. Cachazo, B. Feng and E. Witten, *Direct proof of the tree-level scattering amplitude recursion relation in Yang-Mills theory*, Phys. Rev. Lett. **94**, 181602 (2005), doi:10.1103/PhysRevLett.94.181602.

[8] C. Even-Zohar, T. Lakrec and R. J. Tessler, *The amplituhedron BCFW triangulation*, (arXiv preprint) doi:10.48550/arXiv.2112.02703.

[9] N. Arkani-Hamed, F. Cachazo, C. Cheung and J. Kaplan, *A duality for the S matrix*, J. High Energy Phys. **03**, 020 (2010), doi:10.1007/JHEP03(2010)020.

[10] N. Arkani-Hamed, Y. Bai and T. Lam, *Positive geometries and canonical forms*, J. High Energy Phys. **11**, 039 (2017), doi:10.1007/JHEP11(2017)039.

[11] G. Dian and P. Heslop, *Amplituhedron-like geometries*, J. High Energy Phys. **11**, 074 (2021), doi:10.1007/JHEP11(2021)074.

[12] P. Galashin and T. Lam, *Parity duality for the amplituhedron*, Compositio Math. **156**, 2207 (2020), doi:10.1112/S0010437X20007411.

[13] F. Mohammadi, L. Monin and M. Parisi, *Triangulations and canonical forms of amplituhedra: A fiber-based approach beyond polytopes*, Commun. Math. Phys. **387**, 927 (2021), doi:10.1007/s00220-021-04160-5.

[14] R. Kojima and C. Langer, *Sign flip triangulations of the amplituhedron*, J. High Energy Phys. **05**, 121 (2020), doi:10.1007/JHEP05(2020)121.

[15] X. Blot and J.-R. Li, *The amplituhedron crossing and winding numbers,* J. Geom. Phys. **193**, 104961 (2023), doi:10.1016/j.geomphys.2023.104961.

[16] S. Franco, D. Galloni, A. Mariotti and J. Trnka, *Anatomy of the amplituhedron*, J. High Energy Phys. **03**, 128 (2015), doi:10.1007/JHEP03(2015)128.

[17] D. Galloni, *Positivity sectors and the amplituhedron*, (arXiv preprint) doi:10.48550/arXiv.1601.02639.

[18] N. Arkani-Hamed, C. Langer, A. Y. Srikant and J. Trnka, *Deep into the amplituhedron: Amplitude singularities at all loops and legs*, Phys. Rev. Lett. **122**, 051601 (2019), doi:10.1103/PhysRevLett.122.051601.

[19] I. A. Aizenberg and A. P. Yuzhakov, *Integral representations and residues in multidimensional complex analysis*, American Mathematical Society, Providence, USA, ISBN 9780821815502 (1983).

[20] B. Eden, P. Heslop and L. Mason, *The correlahedron*, J. High Energy Phys. **09**, 156 (2017), doi:10.1007/JHEP09(2017)156.

[21] C. Langer and A. Y. Srikant, *All-loop cuts from the amplituhedron*, J. High Energy Phys. **04**, 105 (2019), doi:10.1007/JHEP04(2019)105.

[22] J. L. Bourjaily, P. Heslop and V.-V. Tran, *Amplitudes and correlators to ten loops using simple, graphical bootstraps*, J. High Energy Phys. **11**, 125 (2016), doi:10.1007/JHEP11(2016)125.

[23] J. Rao, *4-particle amplituhedron at 3-loop and its Mondrian diagrammatic implication*, J. High Energy Phys. **06**, 038 (2018), doi:10.1007/JHEP06(2018)038.

[24] Y. An, Y. Li, Z. Li and J. Rao, *All-loop Mondrian diagrammatics and 4-particle amplituhedron*, J. High Energy Phys. **06**, 023 (2018), doi:10.1007/JHEP06(2018)023.

[25] J. Rao, *All-loop Mondrian reduction of 4-particle amplituhedron at positive infinity*, Nucl. Phys. B **957**, 115086 (2020), doi:10.1016/j.nuclphysb.2020.115086.

[26] R. Kojima, *Triangulation of 2-loop MHV amplituhedron from sign flips*, J. High Energy Phys. **04**, 085 (2019), doi:10.1007/JHEP04(2019)085.

[27] R. Kojima and J. Rao, *Triangulation-free trivialization of 2-loop MHV amplituhedron*, J. High Energy Phys. **10**, 140 (2020), doi:10.1007/JHEP10(2020)140.

[28] E. Herrmann, C. Langer, J. Trnka and M. Zheng, *Positive geometry, local triangulations, and the dual of the amplituhedron*, J. High Energy Phys. **01**, 035 (2021), doi:10.1007/JHEP01(2021)035.

[29] L. Mason and D. Skinner, *Dual superconformal invariance, momentum twistors and Grassmannians*, J. High Energy Phys. **11**, 045 (2009), doi:10.1088/1126-6708/2009/11/045.

[30] N. Arkani-Hamed, J. Henn and J. Trnka, *Nonperturbative negative geometries: Amplitudes at strong coupling and the amplituhedron*, J. High Energy Phys. **03**, 108 (2022), doi:10.1007/JHEP03(2022)108.

[31] D. Damgaard, L. Ferro, T. Lukowski and M. Parisi, *The momentum amplituhedron*, J. High Energy Phys. **08**, 042 (2019), doi:10.1007/JHEP08(2019)042.

[32] T. Łukowski and R. Moerman, *Boundaries of the amplituhedron with amplituhedronBoundaries*, Comput. Phys. Commun. **259**, 107653 (2021), doi:10.1016/j.cpc.2020.107653.

[33] L. Ferro, T. Łukowski and R. Moerman, *From momentum amplituhedron boundaries to amplitude singularities and back*, J. High Energy Phys. **07**, 201 (2020), doi:10.1007/JHEP07(2020)201.

[34] R. Moerman and L. K. Williams, *Grass trees and forests: Enumeration of Grassmannian trees and forests, with applications to the momentum amplituhedron*, (arXiv preprint) doi:10.48550/arXiv.2112.02061.

[35] N. Arkani-Hamed, J. L. Bourjaily, F. Cachazo, A. Postnikov and J. Trnka, *On-shell structures of MHV amplitudes beyond the planar limit*, J. High Energy Phys. **06**, 179 (2015), doi:10.1007/JHEP06(2015)179.

[36] D. Damgaard, L. Ferro, T. Łukowski and R. Moerman, *Kleiss-Kuijf relations from momentum amplituhedron geometry*, J. High Energy Phys. **07**, 111 (2021), doi:10.1007/JHEP07(2021)111.

[37] S. He, C.-K. Kuo and Y.-Q. Zhang, *The momentum amplituhedron of SYM and ABJM from twistor-string maps*, J. High Energy Phys. **02**, 148 (2022), doi:10.1007/JHEP02(2022)148.

[38] Y.-t. Huang, R. Kojima, C. Wen and S.-Q. Zhang, *The orthogonal momentum amplituhedron and ABJM amplitudes*, J. High Energy Phys. **01**, 141 (2022), doi:10.1007/JHEP01(2022)141.

[39] L. Ferro and R. Moerman, *The Grassmannian for celestial superamplitudes*, J. High Energy Phys. **11**, 187 (2021), doi:10.1007/JHEP11(2021)187.

[40] N. Arkani-Hamed, S. He, G. Salvatori and H. Thomas, *Causal diamonds, cluster polytopes and scattering amplitudes*, J. High Energy Phys. **11**, 049 (2022), doi:10.1007/JHEP11(2022)049.

[41] N. Arkani-Hamed, A. Hillman and S. Mizera, *Feynman polytopes and the tropical geometry of UV and IR divergences*, Phys. Rev. D **105**, 125013 (2022), doi:10.1103/PhysRevD.105.125013.

[42] R. R. John, R. Kojima and S. Mahato, *Weights, recursion relations and projective triangulations for positive geometry of scalar theories*, J. High Energy Phys. **10**, 037 (2020), doi:10.1007/JHEP10(2020)037.

[43] M. Jagadale and A. Laddha, *Towards positive geometries of massive scalar field theories*, (arXiv preprint) doi:10.48550/arXiv.2206.07979.

[44] T. Łukowski, R. Moerman and J. Stalknecht, *Pushforwards via scattering equations with applications to positive geometries*, J. High Energy Phys. **10**, 003 (2022), doi:10.1007/JHEP10(2022)003.

[45] N. Arkani-Hamed, P. Benincasa and A. Postnikov, *Cosmological polytopes and the wavefunction of the Universe*, (arXiv preprint) doi:10.48550/arXiv.1709.02813.

[46] P. Benincasa, *Amplitudes meet cosmology: A (scalar) primer*, Int. J. Mod. Phys. A **37**, 2230010 (2022), doi:10.1142/S0217751X22300101.